

# Final Report

Phase I Study

Primary Objective Grating Astronomical Telescope

August 20, 2007

NASA Institute of Advanced Concepts (NIAC)  
Research sub-award No. 07605-003-060

Thomas D. Ditto

DeWitt Brothers Tool Company, Inc.  
237 Lafayette St.  
New York, NY 10012

Research Laboratory  
DeWitt Pond Lane  
P.O. Box 10  
Ancramdale, NY 12503  
3D@taconic.net



Table of Contents.....	2
<b>Executive Summary.....</b>	<b>3</b>
1. Motivation	
a. Mirrors.....	5
b. Spectroscopy.....	6
c. Infrastructure.....	8
2. Innovation	
a. Features of diffraction gratings .....	9
b. Primary Objective Grating and matched secondary.....	10
c. Data Reduction.....	11
3. Examination	
a. Ground-based.....	12
b. Space-based.....	14
i. Flatness tolerance of a membrane.....	14
ii. Phase tolerance.....	18
iii. Stations.....	19
c. Lunar-based.....	21
d. Sizing the primary.....	23
e. Optimizing grazing exodus.....	26
f. Sensitivity and sensibility of the POG .....	33
4. Experimentation.....	35
a. Angular and spectral resolution .....	35
b. POG efficiency.....	41
c. Flatness tolerance.....	42
5. Recommendations.....	43
References.....	44

## EXECUTIVE SUMMARY

It has been 370 years since a seventeenth century French mathematician, Mersenne, presciently sketched out an astronomical telescope based on dual parabolic reflectors. Since that time the concept of the primary objective has been virtually unchanged. Now a new class of astronomical telescope with a **primary objective grating** (POG) has been studied as an alternative. The POG competes with mirrors, in part, because diffraction gratings provide the very chromatic dispersion that mirrors defeat. The resulting telescope deals effectively with long-standing restrictions on **multiple object spectroscopy** (MOS). Other potential benefits include unprecedented apertures and collection areas. The new design also favors space deployment as a gossamer membrane.

The inventor, Tom Ditto, first discovered that higher-order diffraction images contain hidden depth cues, for which he was granted a seminal range finding patent in 1987. Subsequently, he invented and patented 3D localizers, profilometers and microscopes using POGs. His POG telescope was placed in the public domain to expedite its research.

The function of a telescope's primary objective is to collect flux and to deliver images. Both functions dictate that size matters, and bigger is better. For that reason, there has been a steady push over the past century to ramp up the size of the primary mirror. However, for every doubling of mirror diameter, the elapsed time between initial effort and "first light" has also doubled. Meanwhile, costs escalated beyond the mirror alone, because larger instruments required larger enclosures and better pointing mechanisms.

One key catalog of observation, spectrographic data, is far more difficult to amass than two-dimensional imagery. While the number of observable objects has increased with mirror size, the capacity to take spectra has not increased proportionately. In the best of circumstances, spectrograms are available for one per cent of the all objects surveyed.

Spectroscopy was a historical afterthought introduced in the nineteenth century shortly after the invention of the diffraction grating and well over a century after Newton's 1670 telescope. Spectroscopy is generally accomplished using a diffraction grating as the disperser in the secondary. The light being delivered to the spectrograph is first captured by a primary mirror which provides no chromatic magnification by itself. Sizeable spectrographs could not be deployed while diffraction gratings were rare commodities scribed using mechanical ruling engines that produced one grating line at a time.

Today diffraction gratings are commonplace. Their recent availability is a product of both the invention of holography and the mass replication of surface microstructures. Holography permits all lines in a grating to be made simultaneously in a single photographic exposure. Holograms can then be reproduced by embossing processes. The improvement in replication is analogous to how Gutenberg changed the availability of books. The masters may be expensive, but the copies are not. Computer science is another technology that emerged in the second half of the twentieth century without which our proposed spectrographic instrument could not function due to the complexity of image processing and the large amount of storage required in data reduction.

The employment of very large diffraction gratings as primary objectives for astronomical telescopes requires a novel secondary optical train, much as the invention of the first telescope was premised on the invention of secondary objectives. The POG secondary may consist of a conventional spectrographic telescope placed at an angle of grazing exodus relative to a plane diffraction grating. This *Report* also proposes a holographic POG and secondary spectrograph without any mirrors at all.

Since its initial publication in 2002, through its NIAC Phase I jury review and also four disclosures in SPIE conference technical papers<sup>1</sup>; the first principles behind the novel POG telescope under study have never been seriously disputed. It works like this:

First-order diffraction images appear at angles of grazing exodus relative to a flat POG. The wavelengths presented to the secondary have been diffracted on the basis of their angle of incidence, so an arc above the primary is acquired by wave length selection. Over time, each object appears at a secondary spectrometer slit in a sequence spanning that portion of its spectrum bracketed by the free spectral range of the POG. At the secondary, all objects in view of the telescope are assembled into their continuous spectra during an observation cycle. For ground-based versions, the arc is the line of right ascension, and the cycle is one night. Space-based versions complete a 360° scan with a temporal span based on their inertial guidance.

This new telescope breaks down critical roadblocks standing in the path of very large telescope development. For ground-based instruments, the grating is extensible to kilometer length, because the enclosure is flat to the ground and the moving platform is the ground itself, either the earth or the moon. In space deployment, the primary is flat and can be made from a gossamer membrane which is delivered on a roll and deployed as a ribbon. In both instances, ground- and space-deployment, all data received in any observation cycle are entirely spectrographic. MOS performance is millions of objects.

Our NIAC Phase I theoretical study addresses efficiency and linked parameter interactions which are considered potential show stoppers. We have shown that the new method is robust with regard to substrate flatness but is vulnerable to errors in pitch spacing. We have studied the interrelated parameters of grating length, grazing angles, grating efficiency and integration times. We empirically corroborated first principles. A small grating was used in a bench setup that simulates precession. Wavelength selection was demonstrated. The angles of incidence were shown to correlate to the mathematical models which predicted the telescope's behavior.

NASA has a strong interest in telescope technologies, not only for astronomy, but also for protection of the earth. Be it to find exoplanets, detection of nearby objects in earth orbit crossings, or to study our planet from space, this telescope design has a place in NASA's pursuits. Regrettably NASA closed down NIAC, precluding a Phase II proposal, but the loss of Phase II opportunity resulted in months of cost-free extended study preparing this Phase I *Report*. Based on this *Report*, the concept has been presented to the AFOSR for its consideration under a three year program of basic science research.

## 1. Motivation

### a. Mirrors

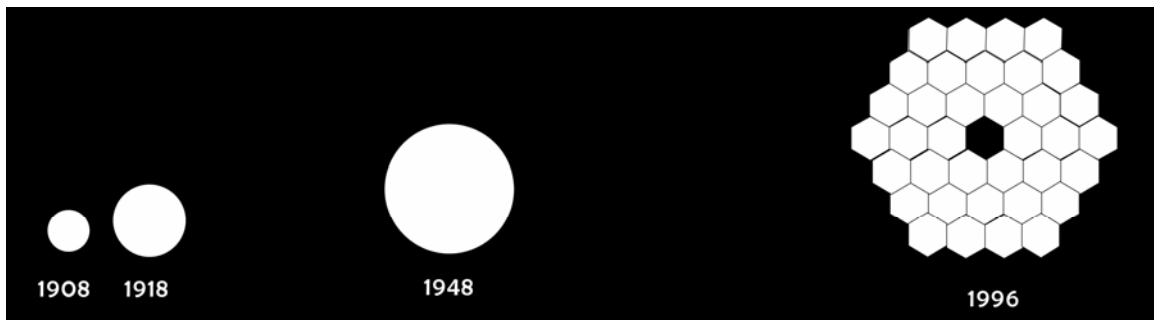


**Fig. 1** 20<sup>th</sup> Century mirrors. Each doubling has taken twice as long as the prior iteration.

Amateur mirror diameters can be in excess of 1 meter, and ten meter-scale mirrors are proliferating in the larger observatories. Some argue that we are on the threshold of a quantum leap in mirror size, but history argues otherwise. In the past century, each landmark step that doubled the size of the primary objective mirror took twice as long as its predecessor. A conservative inference from the historical record is that a jump from 10 meters to 20 meters will not occur with absolute certainty until the end of this century.

Size alone does not determine the performance of a mirror primary objective, because resolution is tied to quality. Smaller mirrors that have been polished to exacting tolerances are the backbone of contemporary science, because it is far easier to fabricate smaller mirrors near to their diffraction limit. Moreover, the largest mirrors suffer from longer slew rates that limit repositioning. A class of agile telescopes has been deployed that can segment the sky and assemble mosaics during a night's observations. The **Sloan Digital Sky Survey** (SDSS) is representative.<sup>2</sup> It repositions after ten minute integration periods. Other agile telescopes are used to track orbital targets which pass overhead at ten times the speed of the firmament. The Maui Space Surveillance System<sup>3</sup> tracks satellites. Although bigger is better under some criteria, small is beautiful under others.

Scale also comes into play when designing space telescopes. A mirror within the diameter of the payload bay or rocket fairing can be stowed with relative ease, and the Hubble Space Telescope<sup>4</sup>, at 2.4 meters, is a case in point. However, as soon as the scale exceeds this diameter, the logistical problem changes character. The telescope cannot be made on the ground and orbited intact. To fabricate a faceted mirror in space presents a robotics problem being addressed by the 6.5 meter James Webb Space Telescope.<sup>5</sup> It will self-assemble on route to the Lagrange point, L-2. Its mirror is made of a beryllium substrate which is lightweight, 15 kg/m<sup>2</sup>, but ancillary structural components raise the gross weight considerably. This compares with a goal of 1.1 kg/ m<sup>2</sup> for ultra-light weight space telescope primary objectives that is considered a key to the feasibility of 100 meter space telescopes.<sup>6</sup> One of the greatest benefits of space deployment, no atmospheric distortion, cannot be fully exploited until space telescopes have primary objectives commensurate in size with the improvement in viewing afforded by space deployment.

## b. Spectroscopy

By 1820 Joseph von Fraunhofer demonstrated that the sun has spectral absorption lines. Astronomers took the observation to heart, because they could thereby gather information about stellar objects that appear as mere point sources in a focal plane image. Spectra reveal the composition and velocity of objects, and from these data the objects can be compared with each other and positioned in a four dimensional universe.

Spectrometers can be stationed at the prime focus of a conventional telescope. The spectrometer has its slit extended to bracket the target and limited in extension to exclude competing objects. This basic configuration allows only as single spectrum of a selected source to be taken during an observation cycle. Adjacent objects are masked out.

However, when sizeable gratings became available, a **primary objective grating** (POG) was deployed in front of the telescope. A lens or mirror concentrated the flux, but the energy was first dispersed by a grating in front of the concentrator. This configuration enjoyed the benefit that adjacent objects were not excluded from the recorded image. All objects were dispersed into spectra at the same time (Fig. 2).

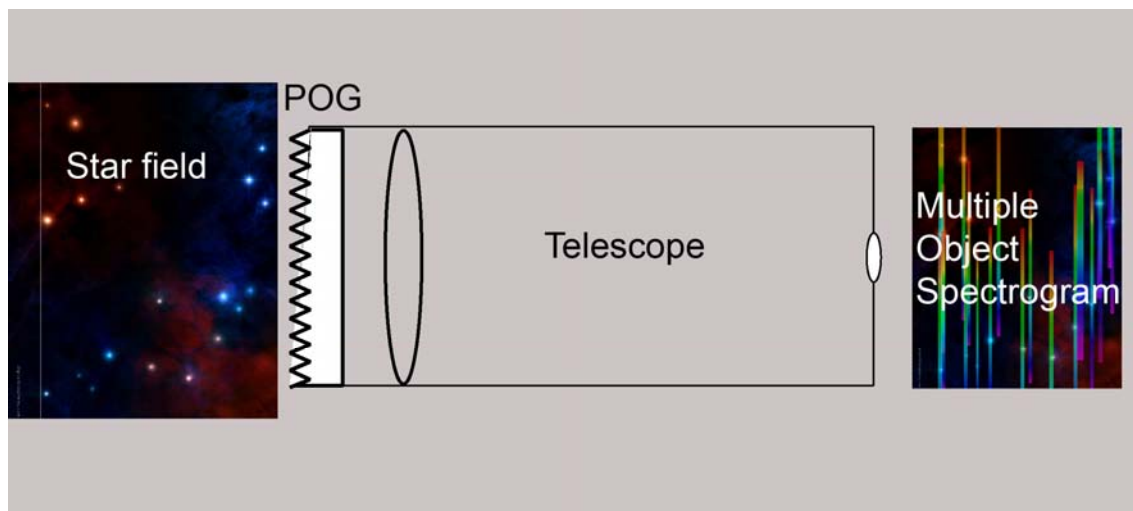


**Fig. 2** Diagram of the Primary Objective Grating (POG) Telescope *circa* 1890

However, the POG telescope had faults that proved fatal to general adoption. The resolution of the acquired spectra was very low, because the entire spectrum had to fall within the field-of-view of the primary mirror, typically less than  $1^\circ$ . As a result, extremely coarse objective gratings were mandatory, and these did not contain the plethora of absorption line data that makes spectroscopy most useful. Secondly, the spectra of all objects in the field-of-view were superimposed on top of each other. The data were ambiguous in regions of superimposition. Even with isolated targets, the sky background formed a noise floor which limited the precise measurement of target flux.

The need for a **multiple-object spectrometer** (MOS) has been growing since the primary objective grating telescope was largely discredited. Because the spectrograph was

considered as the final step in the optical chain, it was assumed that a MOS would contain an image slicer that redirected the two dimensional image formed at prime focus. The images of objects were segregated for acquisition as individual spectrograms.

The putative record holder for the most spectra taken in a single night is held by SDSS. Capable of taking up to 590 target spectra in a single 90 minute observation cycle, a ten cycle night produced 5,760.<sup>7</sup> The targets were pre-designated, and each one had its position drilled into one of ten unique meter-scale aluminum plates. Fibers were inserted at the position of each target, and a 150 kg fiber cartridge for each group was ready on demand. The SDSS MOS has a dual grism design that nominally achieves resolving power  $R=2000$ . (By way of contrast, high-end Echelle spectrographs can achieve  $R=100,000$ .) Alternative spectrographs have been grafted onto the SDSS MOS cartridge,

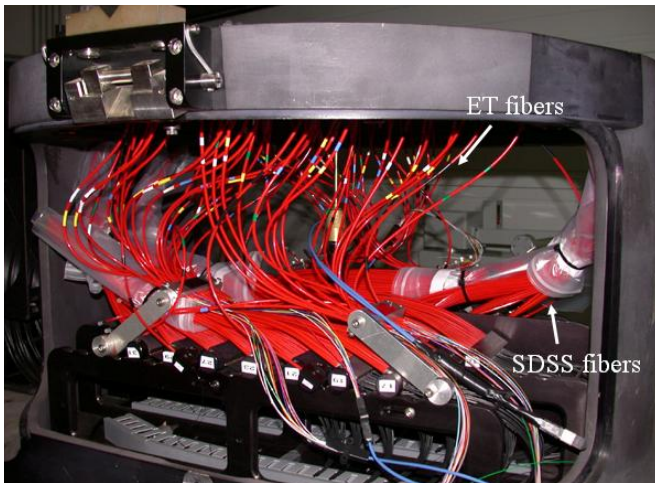


**Fig. 3** Loaded SDSS MOS Fiber Cartridge

because the fibers can deliver selected targets to any secondary instrument. A Doppler interferometer for planet detection<sup>8</sup> is shown in Figure 3. Afterthought has afterthoughts.

Central to the SDSS catalog of spectrograms is a pre-existing catalog of targets taken earlier with four band filters. The selection of targets for spectroscopy can be made with algorithms that examine these coarse color images by rummaging through all

candidates to elect a few for the higher resolving power spectrographic survey. Not only is the physical spectrometer design a late comer in the telescope's history, but the scheduling of spectrograms is itself an afterthought. Discoveries begin with two-dimensional images. Educated guesses follow. Candidates selected by this process are a fraction of the possible targets. In the end, the goal of the SDSS project is to augment its entire survey with spectrograms of one in 100. Given the importance of spectrographic data, it can be said that the Sloan Survey will be incomplete even after achieving its goal of cataloging 100 million objects. 99 million will remain to be seen spectrographically.

There would be advantages to acquiring all objects spectrographically first, if that was possible. Discoveries dependent on spectra should rationally occur in the first pass rather than through the hit and miss process of guessing which objects to schedule for spectrographic study. For example, the sinusoidal Doppler shifts of stars that are used in searches for their planetary systems would be expedited considerably by assembling complete spectra for every object in the field-of-view rather than try and guess which stars are wobbling. The spectrographic resolving power of the survey instrument should be determined by the noise limit imposed by the stellar targets rather than by inherent limitations in the telescope taking spectra.

### c. Infrastructure

The classic telescope dome can be regarded as an integral part of the instrument, because it has unique features. The dome pivots on its base as the stars transit, and it protects the interior, notwithstanding an open roof. The temperature gradients inside the building and between the building and the exterior atmosphere must be minimized. Designing these enclosures requires thoughtful engineering and deep pockets. Construction is an expense that grows as the cube of the telescope tube's length. Due to this expense, there has been a tendency to select low f-numbers for the primary mirror so that the telescope will be as short as possible. Low f-numbers also provide wider views of the sky, but there are unavoidable trade-offs. Most notably, the sizes of the sensor pixels at prime focus are necessarily small, limiting well sizes for photon collection. Also, the figure of the primary must come closer to the diffraction limit compared to allowable tolerances for identical targets at longer focal lengths. These characteristics of short focal lengths are not always desirable, yet the enclosure dictates this optical parameter of the telescope.

Like the enclosure that houses it, the mechanical superstructure of a telescope pivots to track the transit of the stars, but the accuracy required of the superstructure is orders of magnitude more demanding than an active enclosure. Thus the cost for the frame as well as its complex of motors and thrust bearings grows in complexity and in cost close to the fourth power as a function of mirror diameter. One key benefit of enlarging the primary – the increased optical resolution - is defeated by non-compliant tracking mechanisms. At the same time, the increased diameter and weight of the primary objective challenges the load bearing capacity of the structure. To stabilize the superstructure, struts multiply in number and interrupt the wavefront striking the primary. The resulting shadow artifacts lower the effective collecting power and induce diffraction that lowers the resolution.

In an abundance of optimism at the turn of this century, many large scale telescopes had been proposed. The Euro 50 design<sup>9</sup> was modeled using a conventional sliding door roof. Despite the simplicity of its enclosure design, the cost was predicted to equal the cost of the 50 meter primary mirror itself. Computer modeling then showed that the interior of the building was subject to unacceptable gradients of wind and temperature that could not be overcome even with compensation by means of an active superstructure. The project was abandoned. The 100 meter OWL<sup>10</sup> was so large that a dome could not be designed to protect it during use. A rigid superstructure was designed to counter the effects of the outdoor environment. The truss work was extremely dense, casting shadows on the large primary and limiting its potential to collect and focus light. While the projected weight of the telescope grew to 1500 metric tons, at the same time, this gargantuan instrument had to be dynamically guided to tolerances that were measurable in hundredths of arc seconds. Like the Euro-50, the OWL was abandoned. Now there is a 42 meter scale telescope<sup>11</sup> being considered by a consortium drawn from both of these groups. The smaller size is presumably informed by the failure of the larger.

It would seem impossible to invent, but a telescope that was flat to the ground, largely buried underground, and having no moving parts, would seem to offer a path to overcome the limitations that inevitably occur as primary objectives grow in size above 10 meters.

## 2. The Innovation

There are only three known choices for redirecting periodic electromagnetic radiation: refraction, reflection and diffraction. The latter has never been selected as a primary objective because diffraction gratings create unacceptable levels of chromatic dispersion. Even the lesser amount of chromatic aberration caused by refraction led to the virtual abandonment of lenses as primary objectives for large scientific astronomical telescopes.

### a. Features of diffraction gratings

A diffraction grating primary optic was not even a possibility until centuries after the alternatives, lenses and mirrors. In the visible spectrum, diffraction gratings rarely occur in nature. The first diffraction grating recorded in the literature was David Rittenhouse's 1785 invention made by winding a fiber on fine screw threads. The concept was independently reinvented by Fraunhofer in 1819. Ruling engines that scribed the grating lines were then developed in the second half of the nineteenth century. Gratings with variable pitch rules were unknown until ruling engines were supplanted by holography in the later twentieth century. Replicas much larger than meter scale are now being made, and astronomical quality at kilometer scale, along at least one dimension, is conceivable.

Surface relief diffraction gratings are microstructures on a substrate. The substrate is many times thicker than the active microstructures themselves, because the grooves are most efficient when they are on the scale of the incident radiation, fractions of a micron in the visible light regime. Plastic membrane gratings are commonplace decorative items.

The principle of operation is based on interference between adjacent grating grooves. Each groove is essentially a point-source radiator. There are discrete angles subtended from the grating plane where reconstruction at any one wavelength is the sum of all the point sources. These peaks of constructive interference, the orders, are given an integer number, either positive or negative, starting with plus or minus one. Image holograms work exclusively in the first-order whereas some scientific coarse gratings called echelles exploit diffraction orders up to 100 where magnification is greatest. Echelle gratings are the most common high performance grating in astronomical spectrographs.

The backbone of the spectrograph has always been plane gratings with equally spaced straight rules. The spectra acquired at angles of incidence and reconstruction greater than  $45^\circ$  are spread out by an anamorphic magnification feature. The magnification is correlated to the angle of reconstruction, so if light is gathered along the grating plane at angles of **grazing exodus**, the spectral spread is far greater than at lower angles of reconstruction.

Anamorphic magnification comes with a trade-off, because the efficiency goes down as the angle of reconstruction approaches  $90^\circ$ . While simple geometric optical analysis shows the magnification feature growing asymptotically toward infinity, the acquired illumination arrives at zero. Additionally, physical optics dictates a limit to the magnification in inverse proportion to the wavelength of the periodic radiation.

### b. Primary Objective Grating (POG) and a matched secondary receiver

Stated limits aside, the ready availability of ribbon shaped plane diffraction gratings extensible to kilometer scale begs contemplation of their use as primary objectives. The collecting area and aperture could be so much larger than any mirror that a practical embodiment would be of interest. By way of comparison, the largest mirrors at the end of the twentieth century enjoyed collection areas approaching 80 square meters. A ribbon shaped grating that was ten meters wide by a kilometer long would be over 100 times larger and enjoy a resolving power (along its considerable length) that was 1,000 times greater than the angular resolution of the largest mirror today. Applying the “bigger is better” criterion, the implied potential has triggered the present investigation.

Like the original seventeenth century telescopes, POG architecture is made possible through the invention of a novel secondary to both receive and disambiguate the energy collected by the primary. In POG architecture, the analogy to a legacy telescope eye piece is a secondary spectrometer. Light originating from a line of right ascension is diffracted sideways by a POG into a secondary parabolic mirror collector that focuses the light onto the slit of the secondary spectrometer. Light originating from a line of right ascension is diffracted sideways by a POG into a secondary parabolic mirror collector that focuses the light onto the slit of the secondary spectrometer.

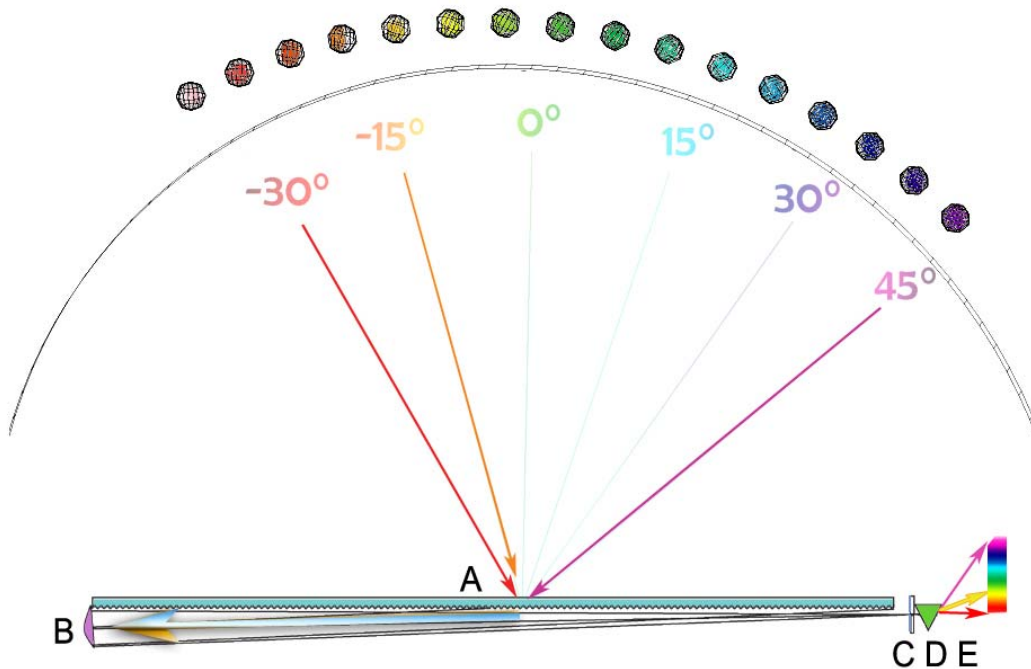


**Fig. 4** Telescope with POG and secondary spectrometer

In any instant of the night, a star at a particular angle is diffracted by POG **A** to secondary parabolic mirror **B**, and the light is focused on slit **C**. A secondary disperser, **D** separates out all the visible objects as spectrum **E**. Three distinct targets at angles  $-30^\circ$ ,  $-15^\circ$  and  $45^\circ$  are illustrated in bold lines, but the entire line of right ascension is covered. As the stars precess their entire spectra are taken over the course of the night.

### c. Data Reduction

The data collected by a POG telescope consists of many snapshots from the spectrograph. This process is distinct from prior art. Most telescopes integrate once for all targets and produce one spectrograph for any target. The POG-based telescope accumulates a series of images and produces a temporal spectrogram by assembling each target at each wave length over the entire observation cycle. In Fig. 5, we see the precession of a star field. A spectrum is superimposed over the precession in the three frames on the left. The output of the spectrograph for the horizontal longitude line is shown on the right hand side. One target is shown at the cross intersection with the vertical latitude line. We see it circled for three frames out of the large number that would be taken over the course of a night.

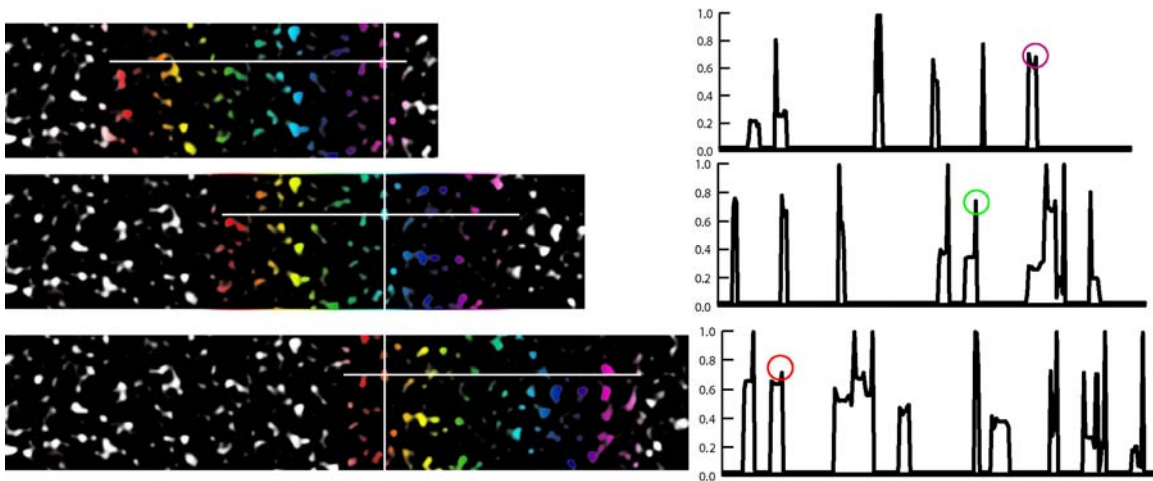


**Fig. 5** Three frames from one night. The crosshairs track one star with circled amplitude.

Computer image processing is required for this type of data reduction, because a very large number of targets are tracked simultaneously over a myriad of frames. The algorithm uses data rotation. A blank table is assembled which has placeholders for each resolved position in the sky. The amplitude of any one wave length is added to the table as it is measured, incremented one placeholder down after each frame.

The number of objects in the field-of-view is a function of the acquired magnitude. The sensitivity of the instrument is a parameter under study, but there is a reasonable expectation that for most latitudes, millions of stars will have their spectra taken in one night. This number far exceeds the most ambitious contemporary MOS by more than three orders of magnitude. In sheer numbers, one night on a POG would equal a decade on the SDSS. Unlike the two step approach of image acquisition during one night followed by spectrograms on later nights, the native output of the POG telescope is spectrographic data, so follow-up spectroscopy is not mandatory.

The outcome is not totally surprising given the premise of using a diffraction grating as the primary collector. The pejorative, “chromatic aberration,” bestowed on diffraction gratings becomes a springboard for an increase in the sheer number of acquired spectra.

### 3. Examination

This innovation leads to many choices for which prior art provides quite limited guidance. The POG telescope may be the best choice for MOS, and it may well be the only choice for a kilometer scale primary objective. The concept can be sketched out for the three key venues: ground-, space-, and lunar-based.

#### a. Ground-based

In the first instance, the telescope could be low to the ground with the secondary optics protected underground. The orientation is strictly east-west, if the unit is to be locked down during observations. Latitude declination could then be set during daylight hours along a single axis of rotation. We illustrate the concept in Fig. 6.

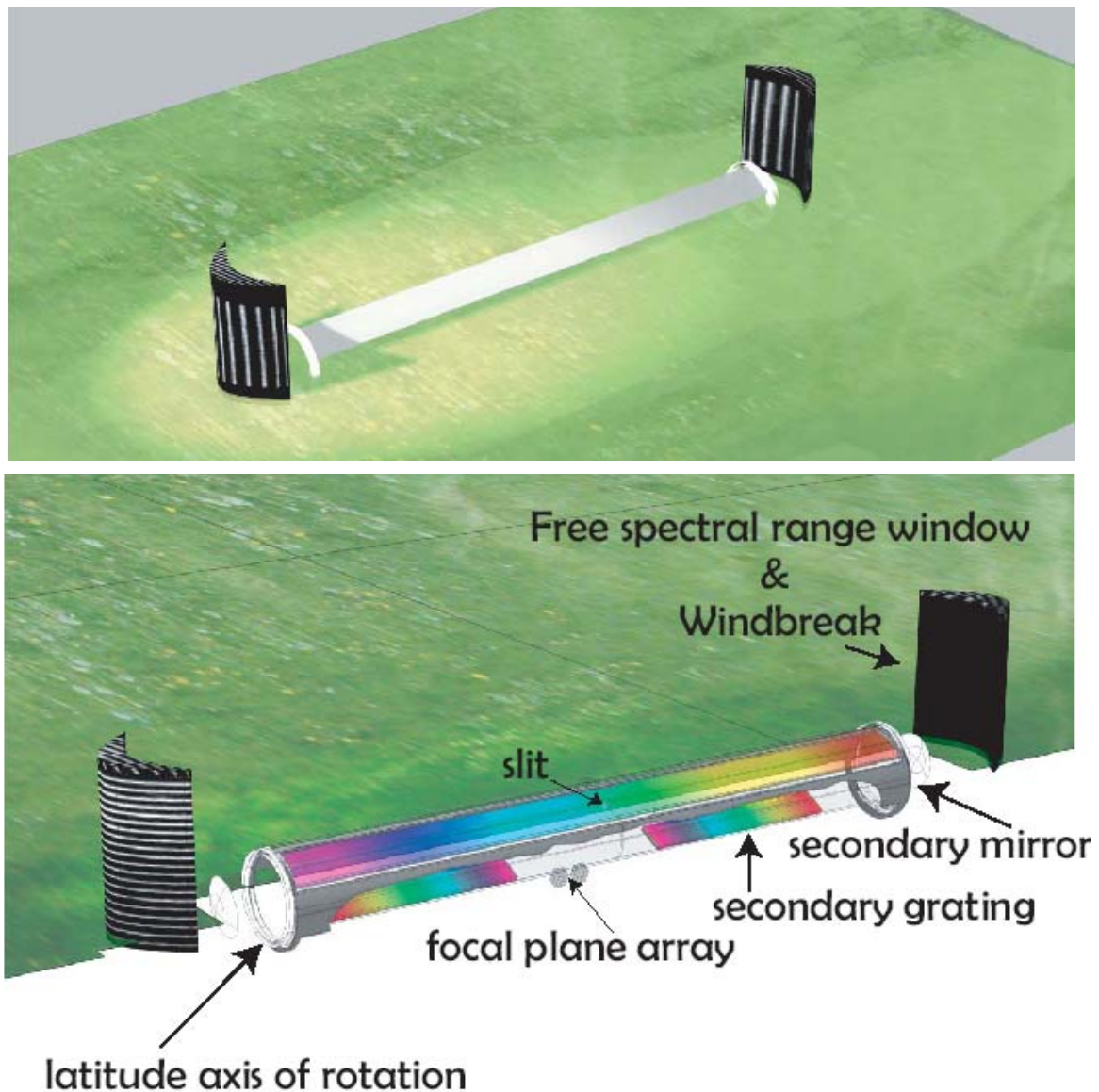


**Fig 6** Ground-based POG Telescope Concept

A notable feature seen in Fig. 6 is the free spectral range window/windbreak. This dual-

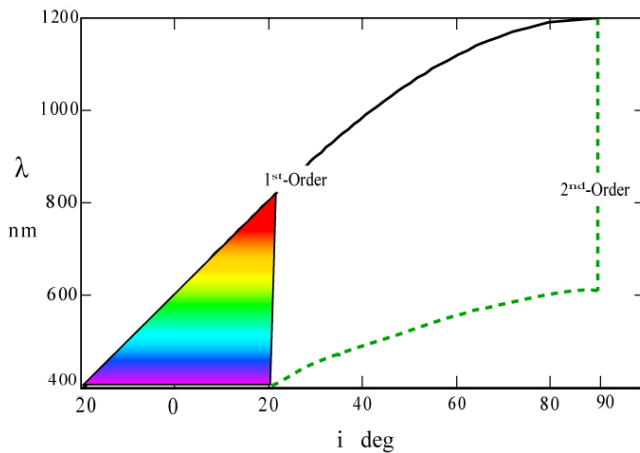


**Fig 7** Free spectral range for 555 nm groove pitch

use baffle lowers wind pressure and (unique to a POG), restricts angles incident on the grating to angles within a free spectral range. The barrier blocks overlapping diffraction orders. As illustrated in the example graphed in Fig. 7 for an 1800 line/mm grating centered on the visible spectrum, the wavelength 555 nm would be seen at  $0^\circ$ , the zenith. To either side,  $\pm 20^\circ$  degrees of the sky would be seen. The second-order above  $20^\circ$  would be masked out.

As conceptualized in Fig.6, a transmission POG is nearly flat to the ground, and the secondary components are buried below in a protected environment within a controlled atmosphere. Temperature gradients can be held steady by sealing this enclosure. End-to-end ray paths need not be interrupted by spiders or other structural support elements. Unlike mirror and lens telescopes, this layout is intrinsically off-axis.

Two mirrors are shown on opposite sides of the primary. This is allowable, because the mirrors would collect the spectra in opposite sequences, as shown in Fig. 8. One benefit in the redundancy is that flux collection is effectively doubled from a single POG.

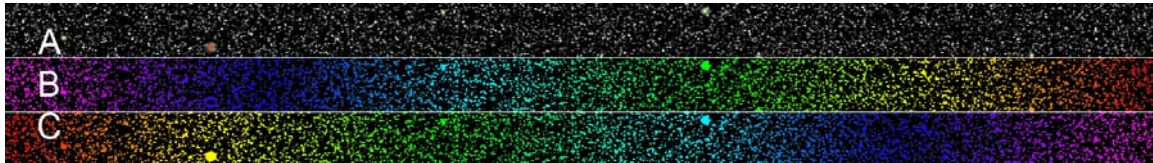


**Fig. 8** Star field A is acquired by opposed mirrors in reverse spectral sequences B and C

The secondary mirrors do not need to move. Also, their focal lengths can be quite long. In the model of Fig. 6, they are half the length of a POG that may be kilometer scale. We discuss POG length in subsection **d.** below, but the focal length restriction of mirror primaries supported by superstructures and contained within domes does not apply here.

Although the POG telescope shares the static pose of the mercury metal liquid mirror telescope (LMT) zenith tube, the POG can be rotated along its considerable length to acquire any latitude. The POG field-of-view is anamorphic. It is restricted to the lateral view of the mirror, but along the axis of diffraction it can be many times greater. In Fig. 7 the model illustrated is for a  $40^\circ$  field-of-view along the line of right ascension. On the other hand, the lateral field-of-view is a function of the secondary mirror. It might be degrees-wide for surveys or arc minutes-narrow for isolating discrete targets.

### b. Space-based

The ribbon-shaped POG lends itself to deployment in space, because it can be stowed as a gossamer membrane transported on a roll. The configuration for stowage conforms to the payload geometry of delivery vehicles. Unlike mirrors which need to be segmented for sizes beyond the diameter of the fairing or payload bay, the ribbon is stored as a continuous integral surface on a drum and is unfurled during deployment.

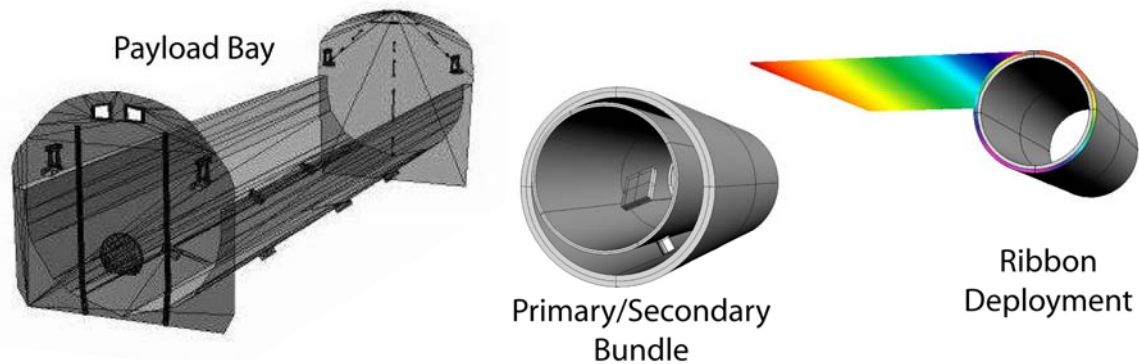


**Fig. 9** POG Stowage and Delivery

Diffraction addresses the conundrum of making a collector from tensile material. We abandon the three dimensional figure. A POG is flat. It also turns out that gratings differ significantly from mirrors with regard to their operational flatness figure tolerances.

### i. Flatness tolerance of a membrane

For a ribbon POG, diffraction occurs along the long axis, while the shorter width is no different than a mirror or refractive flat plate, Fig. 10.

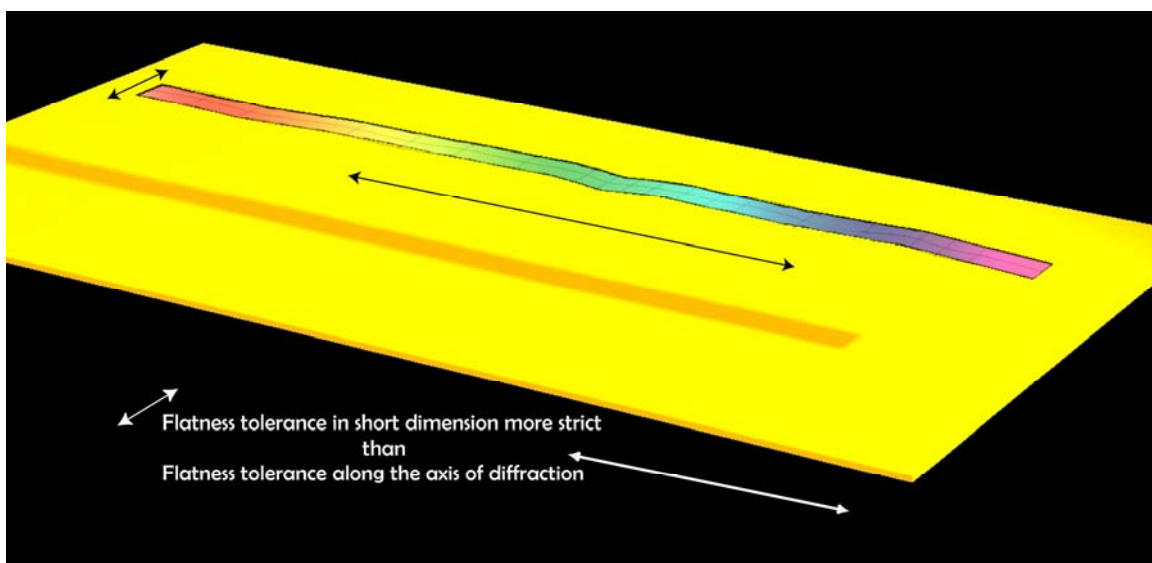


**Fig. 10** Flatness Specification

Two sets of equations are required to establish tolerances. We have investigated the flatness tolerances for the diffraction grating by using a model that considers the effect of displacement over a considered length.<sup>12</sup> Flat mirror tolerances are in the literature.

We assert that the tolerance for flatness in the diffraction dimension relaxes as the angle of grazing increases. This is because the diffraction image is formed by the constructive sum of in-phase waves originating from all grating grooves. When the light exits along the grating axis, variations in grating height have a negligible effect on the phase of the waves passing nearly parallel to the grating surface and exiting to the side.

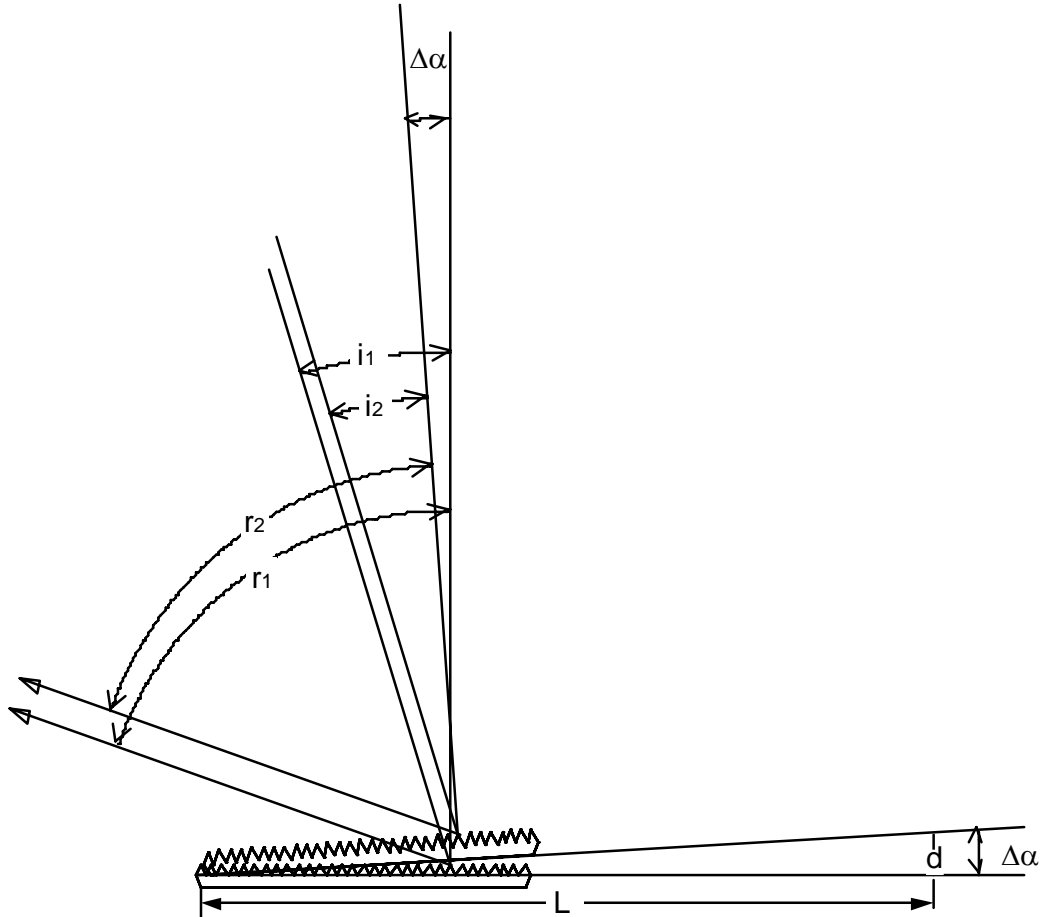


**Fig. 11** Parameterization of flatness tolerance specification

We can approximate the flatness tolerance for grazing exodus by using a displacement  $d$  over considerable length  $L$ . We compare two rays that are rotated by angle  $\Delta\alpha$ .

$$(1) \quad \Delta\alpha = \arctan\left[\frac{d}{L}\right]$$

Angles of incidence  $i_1$  and  $i_2$  are rotated by  $\Delta\alpha$  as are receiving angles  $r_1$  and  $r_2$ . Assuming we have determined incidence and receiving angles, we can compare the

change in wavelength as a function of the surface flatness by calculating two wave lengths.

$$(2) \quad \Delta\lambda = \Delta\lambda_1 - \Delta\lambda_2$$

where  $\Delta\lambda$  is the spectral resolution and  $\lambda$  is determined by the Diffraction Equation:

$$(3) \quad \lambda = \frac{(\sin(i) + \sin(r))}{n} p$$

where:

$\lambda$  = wave length of radiation

$i$  = incident angle

$r$  = receiving angle

$p$  = grating period

$n$  = diffraction order

We are examining incident radiation arriving near the zenith. This analysis suggests that when flatness is held to the same tolerance as the SDSS mirror, 100 nm over 2.5 m, the spectral resolution of the grating  $\Delta\lambda$  in its worst case at the zenith is 0.000025 nm. When the light is at both grazing incidence and grazing exodus, there is no phase delay regardless of surface irregularity, and  $\Delta\lambda \rightarrow 0$ . In existing practice, surface tolerance is well appreciated by diffraction grating manufacturers who use float glass as a substrate where Ångstrom resolution is specified.

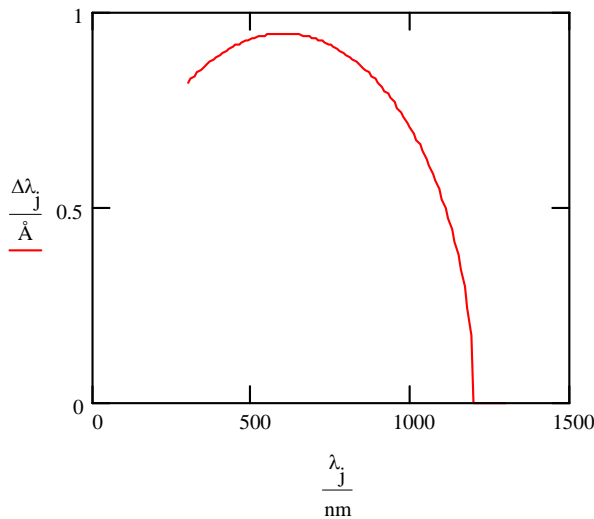


**Figure 12** Ångstrom resolution with garden variety float glass rated at 8 waves per inch supporting a 600 nm grating configured at grazing exodus  $r = 88^\circ$

We plot a relationship of  $\lambda$  vs.  $\Delta\lambda$  in Fig. 12 where the substrate is a modest quality float glass. In the example, exodus angle  $r = 88^\circ$ .

To correlate spectral resolution to angular resolution, we look at the linkage between the two. Small changes in wavelength correspond to small changes in the angle of incidence when the receiving angle  $r$  is fixed. We can determine  $\Delta i$  by taking the difference of the change in  $\lambda$  over one slope direction in the curve. We use Equation. (4).

$$(4) \quad \Delta i = \arcsin\left[\frac{\lambda}{p} - \sin(r)\right] - \arcsin\left[\frac{\lambda - \Delta\lambda}{p} - \arcsin(r)\right]$$

Note that under the presumption of a high frequency grating where the acquisition is exclusively in the first-order, we assume that  $n = 1$  and exclude that term.

Using Eq. (4) we consider another case using a tighter tolerance for grating flatness of 600 nm over 100 m. This tolerance would be considered substandard for mirrors, and yet it certainly represents a challenge for very large membrane structures. The error due to flatness is then shown to be on the order of 0.001 arcsecond, Fig 13. This approximates the angular resolution that will separate an exoplanet from its host star. The theoretical limit for  $\Delta i$  for a grating as measured along the diffraction axis for a POG of 100 m length can also be calculated from the resolving power  $R$  on the basis of the grating length  $L$ :

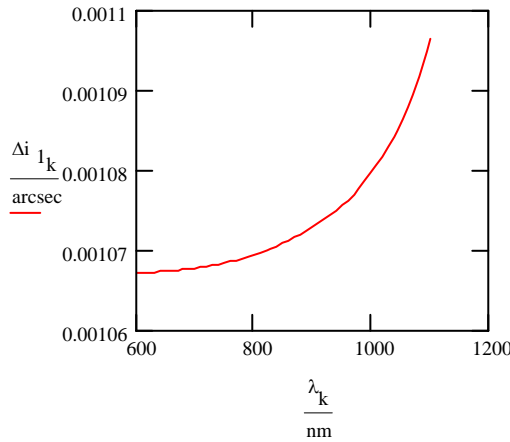


**Fig. 13** Resolved angles from 100 m POG with overall deviation in flatness restricted to ~ 1 wave

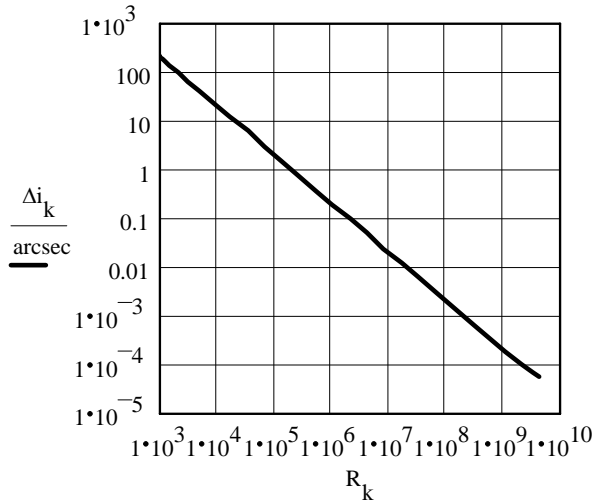


**Fig. 14**  $\Delta i$  as a function of  $R$  using a log scale

$$(5) \quad R = \frac{L}{\lambda}$$

$\Delta\lambda$  can then be known from

$$(6) \quad \Delta\lambda = \frac{\lambda}{R}$$

For 600 nm infrared radiation incident along a 100 m grating,  $R = 1.667 * 10^8$ . The resolving power limit of  $\Delta\lambda$  is  $3.6 * 10^{-5} \text{ \AA}$ . With Eq. (4) we can determine a theoretical limit of  $\Delta i$ . For a 100 m POG,  $p = 600 \text{ nm}$ , we calculate that  $\Delta i = 1.245 \text{ milliarcsecond}$ . We show the generalized relationship at this wavelength for a wider set of first-order resolving powers in Fig. 14. The evidence suggests that if the POG can be kept flat end-to-end to a tolerance that falls within the wavelength of the light it is measuring, the primary objective can achieve a precision of angular resolution performance that is close to the theoretical limit of its resolving power as a diffraction grating.

If this is true, the flatness tolerances for diffraction gratings are different than figure tolerances for mirrors. Designing a space borne POG presents relaxed tolerances for its length as compared with. its considerably narrower width.

In the lateral (short) dimension, the POG is essentially the same as a mirror, and the requisite flatness tolerance is well understood from the simple relationship that the angle of incidence equals the angle of reflection. We leave this analysis to the reader.

Optical flats have been made in membrane materials that reach surface roughness of 20 nm and overall flatness on the 100 nm scale.<sup>13</sup> The cited demonstration was made on a 0.75 meter scale experiment. Extensibility to larger size would seem unimpeded. The underlying physical principle is that tensile membranes want to be flat.

## ii. Phase tolerance

The peak to peak groove phase relationship presents another tolerance problem. Even if the phase error is minimal at manufacture, it can easily be aggravated by conditions after deployment in space. A tensile structure will face stress factors that are both uniform and non-uniform, creating errors, some continuous and others stochastic.

Reworking Eq. 4 to make spacing between rules  $\Delta d$  a variable we set a dependency for  $\Delta i$ .

$$(7) \quad \Delta i = \arcsin\left[\frac{\lambda}{d - \Delta d} - \sin(r)\right] - \arcsin\left[\frac{\lambda}{d} - \arcsin(r)\right]$$

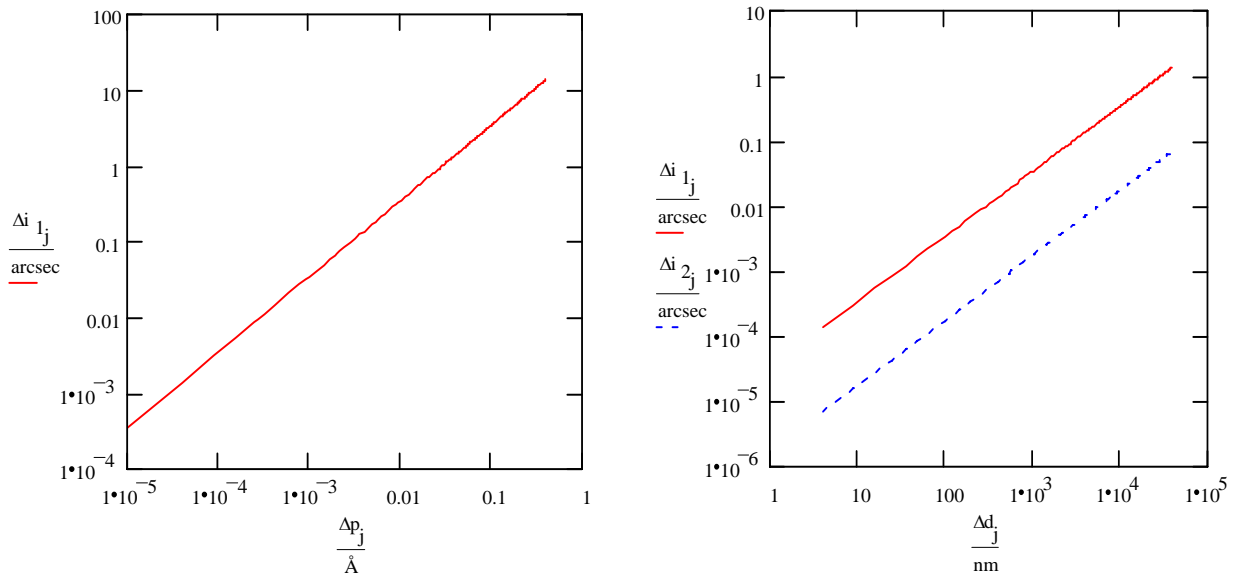
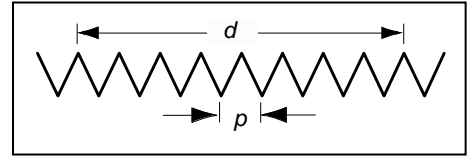
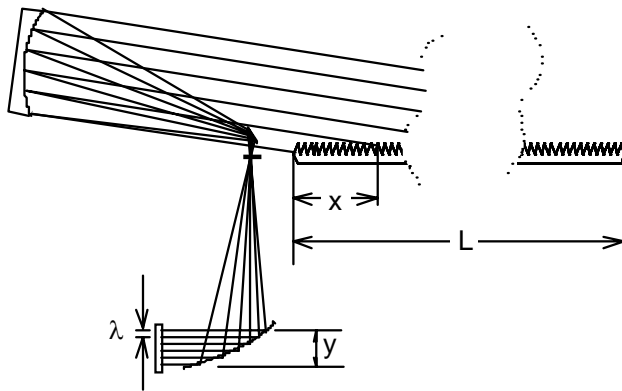


**Fig. 15** (a)  $\Delta i$  for nodes  $p = 600$  nm (b) nodes spaced by  $d = 1$  cm, and  $r = 88^\circ$  &  $r = 45^\circ$ .

We show a result for grazing exodus for a 600 nm pitch grating in Fig. 15 (a). If a grating had only two adjacent grooves, milliarcsecond angular resolution would presume pitch accuracy to approximately the diameter of a proton. However, the resolving power of a diffraction grating is directly proportional to its length. In Fig.(b) 16 we show the phase error for angles of  $\Delta i$  by setting  $d$  to 1 cm. Now  $\Delta d$  is measure in 100's of nm rather than thousandths of  $\text{\AA}$ . We do note the tolerance is less forgiving for angles of grazing exodus.

We made a preliminary analysis that may be heuristically consistent with the result shown in Fig.15 (b) where the phase problem appears to be aggravated by greater angles of  $r$ . While a thorough analysis for this problem has yet to be done, in a prior publication we suggested that a coherence length be taken from the sub-section of a grating required to produce a specific wavelength in the receiver as a fraction of the entire POG length.<sup>14</sup> Ray paths to the collector can be separated from each other in single wave length divisions if the secondary has considerable width. If the secondary is modeled with the considerable length  $y$ , any wave length segment  $\lambda$  can be mapped back to the grating of



length  $L$  to determine the incremental steps  $x$  over which phase error must be within tolerance. The relationship is

$$(8) \quad x = L \frac{\lambda}{y}$$

This relationship is shown in a cross section in Fig. 16. This may explain the tighter tolerances required as  $r$  approaches grazing exodus. More study is required.

**Fig 16** Phase coherence model

We do suspect that an active substrate that can vary its tensile properties, such as the “muscle” membrane investigated contemporaneously with our present research by NIAC Fellow, Joseph Ritter,<sup>15</sup> will become mandatory to buffer the gossamer membrane against stretching and displacements that affect uniform grating pitch.

**iii. Stations**

The pose of a POG deployed in space must vary its incident angles to sequence the wave lengths of the acquired objects. Simple rotation analogous to a radar antenna will provide this requisite angular variation and also inertial stability. We call the embodiment “The Boloscope.” Outboard secondary telescopes create the ballast. The inertial forces provide tension for the membrane.

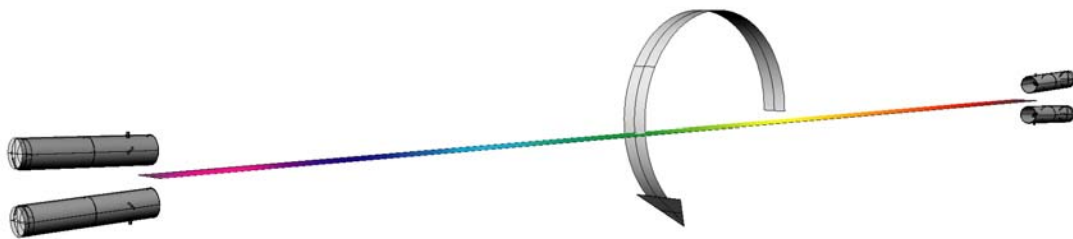


**Fig. 16** “The Boloscope,” a rotating platform, illustrated with symmetrical secondaries

The Boloscope has inertial characteristics anticipated by space tethers. The inertial forces can be modeled using software for space tethers developed by Hoyt, a NIAC Fellow.<sup>16</sup>

To add the intrinsic stiffness of a curved surface while also concentrating flux in the narrow dimension, one option is to create a parabolic trough. The superstructure bears similarity to the Dual Anamorphic Reflector Telescope (DART).<sup>17</sup> The DART was considered for sub-millimeter and deep IR, because it was not expected to hold a figure suitable for visible light, but the trough might have supported a figure suitable for a POG.

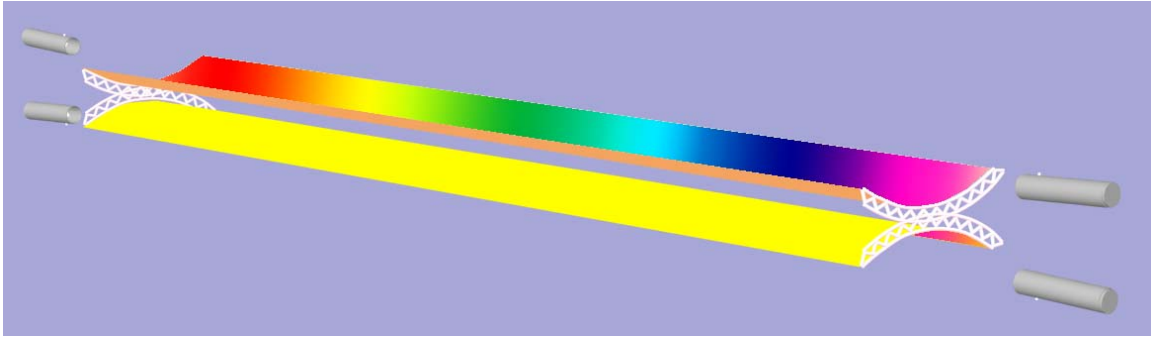


**Fig. 17** A dual parabolic truss superstructure for rigidity

A rigid embodiment would have less need for the Bolo's centrifugal force stabilization. It could enjoy a stationary pose where changes in incident angle were imparted by a gradual orbital rotation around a gravitational center such as the earth, the moon or the sun. This would result in longer integration times and the possibility of narrow bandwidth scanning.

Locations for a POG space telescope could include low earth orbit (LEO) and geostationary orbit (GEO). Their selection might evolve in that sequence over a development period leading to the expertise needed for the LaGrange points.

A LEO tin can experiment would be useful simply to evaluate the POG concept. In full scale, LEO is the most likely station for astronaut service calls. The Hubble Space Telescope proved the value of such an option. In LEO, gravitational attraction toward the center of the earth could be exploited to maintain a vertical pose. This is a relatively static posture that would also simplify docking. Incident angles on the firmament would vary in the same manner as the ground-based version of the instrument with integration times shortened to a much more rapid orbital time scale.

Large primary objective mirrors on the scale of 150 m have been contemplated for GEO insertion as reconnaissance telescopes. Repeating history with Keyhole for reconnaissance and Hubble for astronomy, if the former can be achieved, then the latter will follow. A geostationary reconnaissance telescope would require the large aperture to have meaningful ground resolution, and a POG might prove more practical than the robotic self-assembly and maintenance of a very large mirror.

A hybrid option, diagrammed in Fig. 18, would place a secondary on the ground as a static fixed installation for a POG at GEO. Under this regime, the secondary could be serviced on the ground with relative ease. The scale of the ground-based secondary collector would be unprecedented, in the 100 m class, but as a zenith tube it could rest flatly on a firm foundation. The GEO POG might be on the order of 1 km x 10 m. The

entire instrument could have an optical diffraction limit on the order of 0.001 arcsecond, as is suitable of exoplanet discovery, if adaptive optics were capable of neutralizing the atmosphere for such an enormous secondary mirror aperture on the earth's surface.

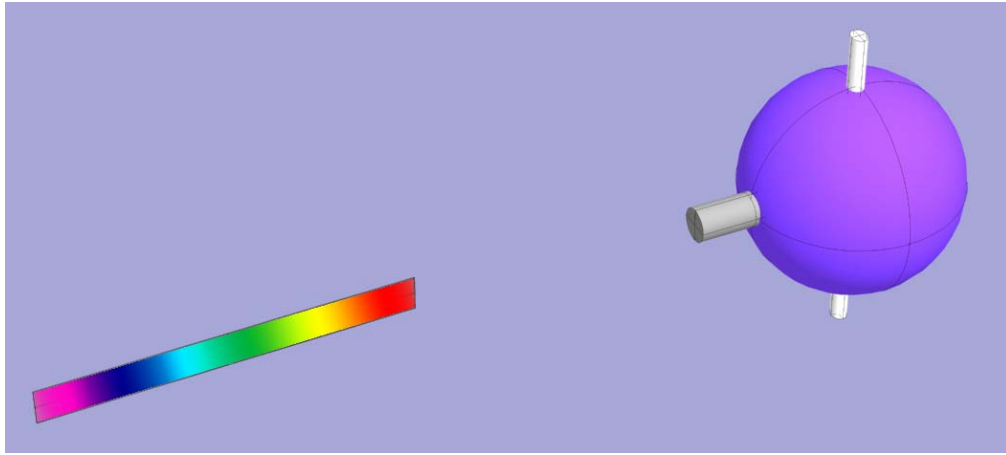


**Fig 18** GEO POG at geostationary and secondary on equator (not to scale)

### c. Lunar-based

Lunar observatories with very long integration periods have been studied by NIAC Fellows Angel and Worden.<sup>18</sup> The benefit of long term observations on fixed swaths of sky are numerous, one being penetration to the farthest reaches of the universe with the potential of resolving long standing questions of galaxy formation after the Dark Ages, about 400,000 years after the Big Bang. The moon, a solid rock inside a vacuum environment with relative proximity to earth, provides an ideal platform for this type of long term experiment. One key to a successful observation would be a telescope that required little maintenance as it gradually accumulated and relayed data.

A POG can be coupled to a secondary spectrometer that is subtended at grazing exodus of  $r = 90^\circ$ . In this special case, the spectrometer is connected to the primary by a wave guide that tunnels diffracted light. The resulting telescope has no moving parts and is sealed to the outside world. It is a “set it and forget it” instrument that could operate for decades with little or no servicing.

The lunar POG is derived from the edge-lit hologram where illumination enters through a base plate and is diffracted toward the observer.<sup>19</sup> The converse is also possible, that is, the illumination can be from the surface normal and exit the optic from the base plate. In this configuration the acquisition will be by a wave length selection according to angle of incidence. This is the POG principle, but the secondary is has no mirror. The base is a light pipe that can trap the incident radiation and conduct it to a secondary where it is delivered at the edge of a plate, Figs 19 & 20. To work, the POG is not a plane grating. It is the hologram of a point source, and it can form an image at a fixed wave length of a target object. For each wave length, the image forms at a different focal length. When focused to one side, the hologram replaces the secondary mirror.

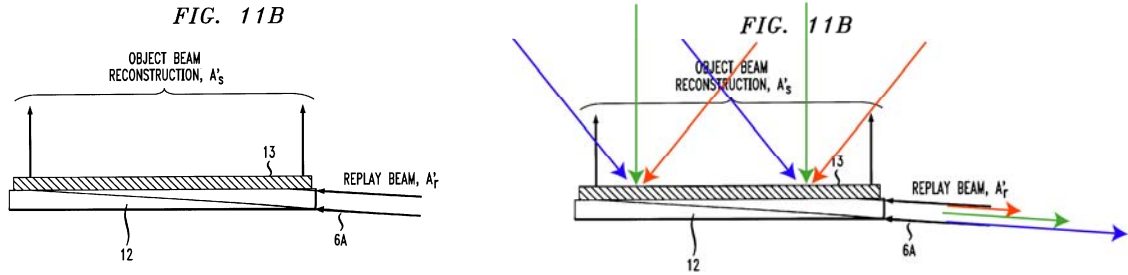


**Fig. 19** POG with light pipe to secondary spectrometer based on the edge lit hologram

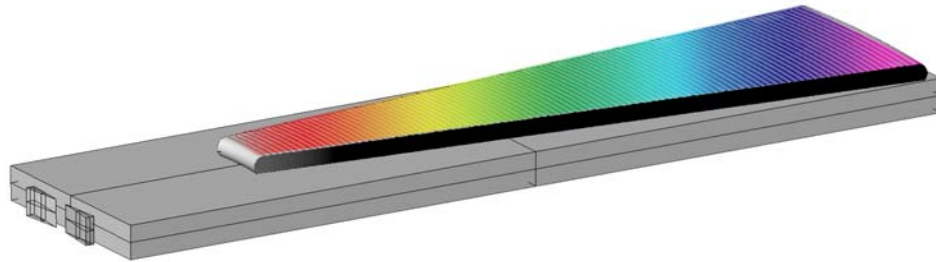


**Fig. 20** Holographic primary collector with variable pitch spacings and curved rules

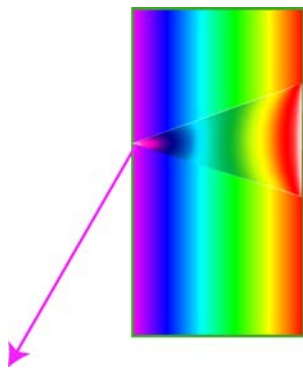


**Fig 21** Bragg Filter Plate - single wave, single star

Extracting the star field requires a complex secondary spectrometer that takes advantage of the concentration of a known wave length at a known position. This secondary plate is a variation on the fiber Bragg grating commonplace in telecommunications. The filter, Fig. 21 disperses a specific wave length and passes others. Mated to the primary where the star field comes into focus, the Bragg filter produces measurable flux at positions corresponding to the line of right ascension and wavelength. In Fig. 21 one wave length for one star is shown diagrammatically. Photo sensors placed at all points above the plate collect all stars at all wavelengths. Fig. 22 shows the entire telescope assembly.

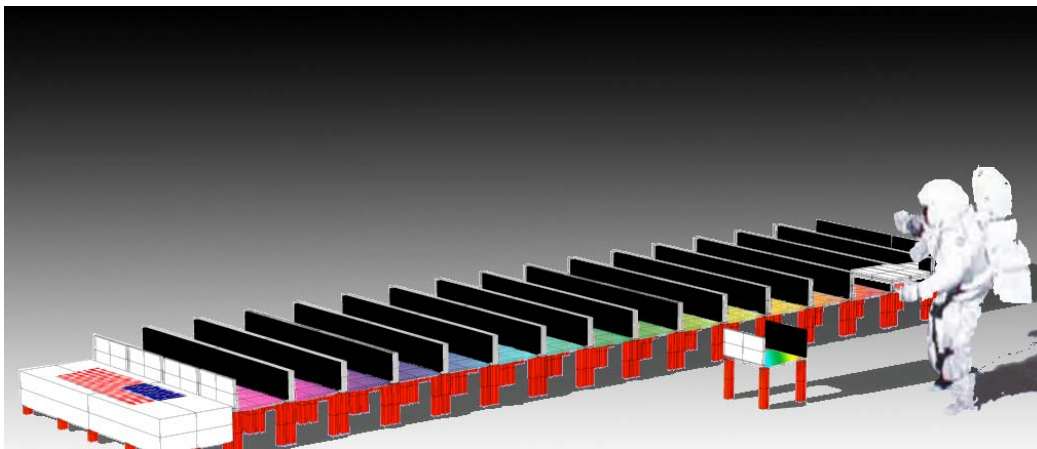


**Fig. 22** Lunar Observatory, covers open; Bragg filter assembly on the left hand side

The lunar POG is modular and is extensible over periodic servicing and upgrades. As illustrated above, each unit is made up of a subsection of a larger hologram, with a base pedestal and dual-use baffles. When opened during the night, the baffles window the first-order and block higher-orders. During the lunar day, they close to protect the POG.

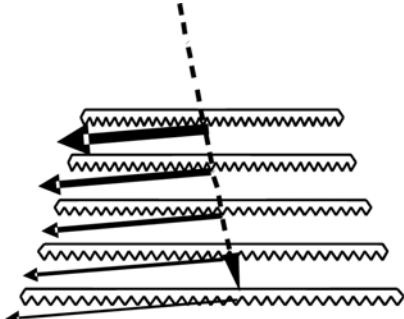


**Fig. 22** Cumulative efficiency with stacked transmission

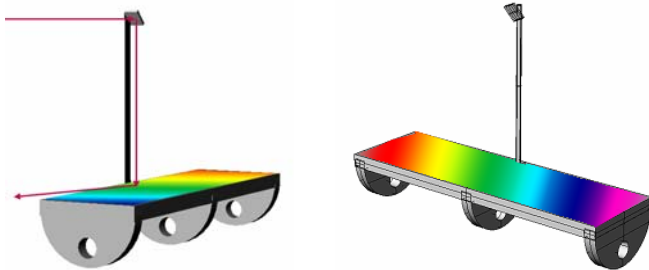
Grating Efficiency =	0.1		
Total flux =	100		
	first-order	zero-order	Effective Efficiency
Layer 1	10	90	10
Layer 2	9	81	19
Layer 3	8.1	72.9	27.1
Layer 4	7.29	65.61	34.39
Layer 5	6.561	59.049	40.951
Layer 6	5.9049	53.1441	46.8559
Layer 7	5.31441	47.82969	52.17031

**Table 1** Multiple layer grating effective efficiency

The POG holograms would be transmission. As a result, grating efficiency can be enhanced if the POG is layered, Fig 22. Zero-order flux passes through a top grating layer and is subjected to subsequent diffraction by lower layers. A nominal 10% efficiency becomes over 50% with seven layers. A sample calculation is shown in Table 1.

**d. Sizing the primary**

In the past, the construction of telescopes from monolithic components resulted in the concept of “first light,” the moment when all the requisite parts of a telescope were used in tandem for the first time. Without near-completion of all the components: the mirror, its superstructure, and the enclosure; it was impossible to begin observations and shake down the instrument. For this reason, an extensible instrument that can be built piecemeal is not typical of large telescope design.



A POG can be segmented. This is particularly true for the ground- and lunar-based embodiments. We have conceptualized discrete flat tables that pivot to observe different latitudes, Fig. 23. Alignment of the gratings resting on the modules is made by piezo stacks that translate the diffraction gratings under guidance from laser interferometers.

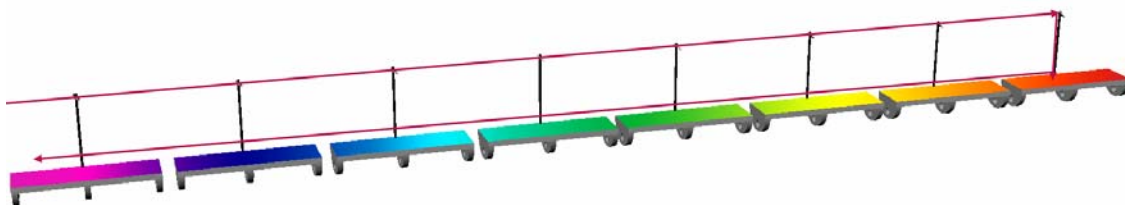


**Fig. 23** Discrete POG modules with ganged laser interferometric alignment masts

The maximum length of the POG  $L$  is determined by the receiving angle  $r$  and the diameter of the secondary mirror  $D$ , Fig. 24. The dependency is

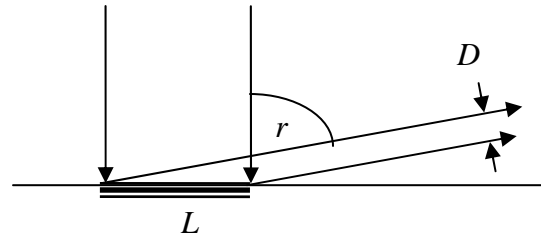


Fig. 24 POG length, mirror dia. and  $r$ .

$$(9) \quad L = \frac{D}{\cos(r)}$$

In the example of Fig. 25, grating lengths up to a kilometer are plotted against mirror diameters. Receiving angles are separately plotted from  $85^\circ$  to  $89^\circ$  in  $1^\circ$  steps.

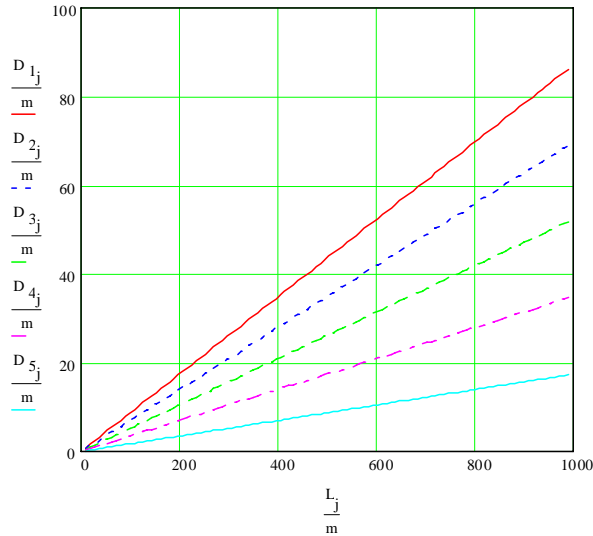


Fig. 25 Diameters needed for lengths to a kilometer

The ratio of the length to the secondary mirror diameter is the anamorphic magnification of the POG.

$$(10) \quad M = \frac{L}{D}$$

The ratio is plotted in Fig. 26 on a log scale for  $r$  between  $85^\circ$  and  $89.4^\circ$ .

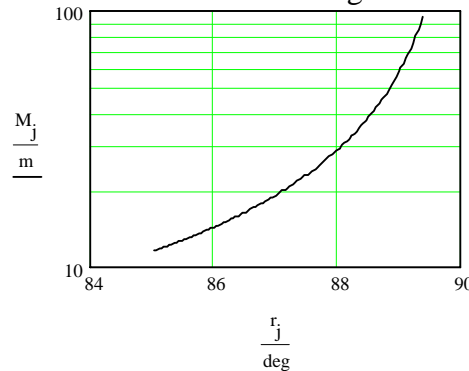


Fig. 26 Magnification as function of  $r$

The magnification is asymptotic to  $r = 90^\circ$  where it is infinite. The length of the POG is then extensible as far as is practicable. For this reason, A POG lunar observatory could be grown during its lifetime if modules are delivered during sequential lunar missions. In principle, if each module is part of a larger hologram, then a module can be inserted at its designated station whenever the whole has grown to the proportion where the module fits. We show the concept as a simplified diagram in Fig. 27. In space, kilometer scale gossamer membranes are not preemptively constrained by aerial mass, as is glass; because a membrane weighs approximately  $100 \text{ grams/m}^2$ .

Drum packaging for insertion conforms to delivery vehicle dimensions. The wrap

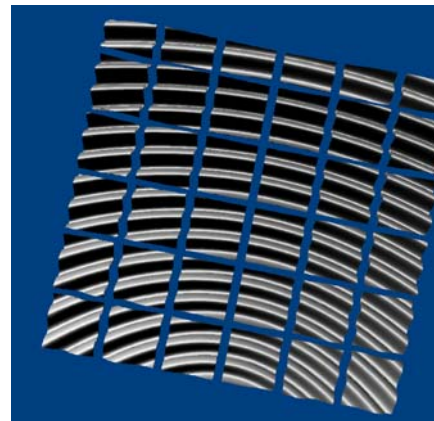
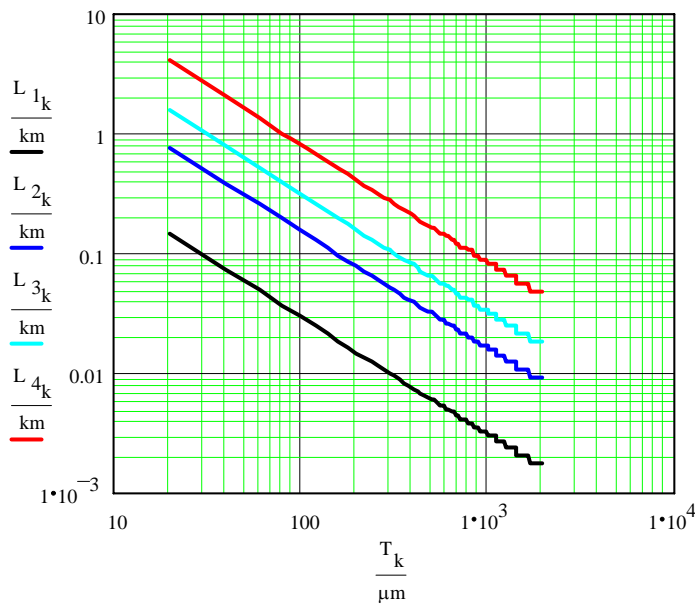


Fig. 27 Segmented hologram

required to hit kilometer length can be calculated by the approximation of



**Fig. 28,** Stowable lengths of membrane

$$(11) \quad L = \sum_{n=0}^N \pi(OD - nT)$$

$OD$  is the outside diameter

$T$  is membrane thickness

$N$  is the number of wraps

$$(12) \quad N = \frac{OD - ID}{T}$$

For a ribbon POG, drum storage during transport could offer optical surface protection without significant mechanical or weight overhead. The tensioning frame could present a mechanical and launch weight problem. Study is needed. We presented a paper at the AIAA seeking collaborators.<sup>20</sup> As a result, we have initiated discussions with Mevicon, Inc.

Perhaps the only possible choice for a kilometer scale primary on the ground will turn out to be the POG. However, is the POG competitive in diameter ranges practical for mirrors? Consider a 10 m mirror and a 10 m short pitch grating where only the first-order reconstructs. Using the Raleigh criterion for performance, the diffraction limited angular resolution of the mirror is 0.015 arc seconds at 600 nm. Equations (4) – (6) above lead us to assert that a 10 m POG could achieve a theoretical angular resolution of 0.0125 arc seconds. The two approaches yield nearly the same angular resolution limit at the same aperture. Equal apertures for both mirror and POG resolve equally.

The similarity ends with angular resolution. The mirror magnifies in two dimensions, and a plane grating is anamorphic. Moreover, it cannot focus anything without a mirror in the secondary. The mismatch becomes an issue, because the lateral resolving power of the secondary mirror is likely to be lower than the longitudinal resolving power of the grating along the axis of diffraction. This is not altogether a problem if the goal is acquisition of spectra, since the imaging and spectral parameters are not the same. However, the secondary spectrograph will have a limit in its resolving power that can nullify the resolving power of the POG.

One avenue of investigation is to design the POG holographically, as illustrated in Fig. 27 where the angular resolution can be equal in both dimension. Holographic POGs would be a productive topic for future investigations into this configuration.

**e. Optimizing grazing exodus**

If gratings and mirrors share similar resolving power as a function of their size, they differ greatly with regard to their collection efficiency. At grazing exodus, the efficiency of a surface relief metalized reflection grating drops precipitously as the grazing angle approaches 90°. In Fig. 29 we show the predicted efficiency of a 555.5 nm reflection grating with a groove depth of 280 nm for grazing angles subtended from 90° to 85°.

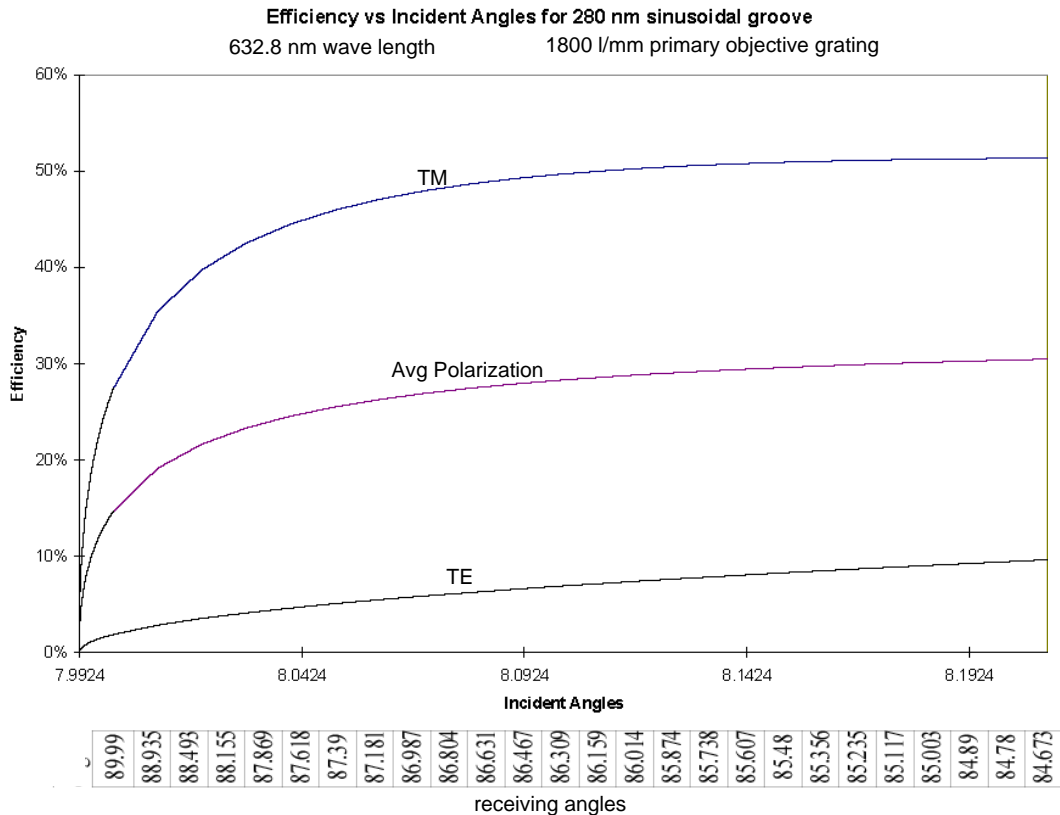


**Fig. 29** PCGrate® prediction of the HeNe line near grazing exodus for a 555.5 nm POG

We also learn that grazing exodus is highly polarizing with the losses in the electric transverse wave reducing the average polarization by half. Even more dramatic are the overall losses regardless of polarization, since the efficiency drops to zero at 90°.

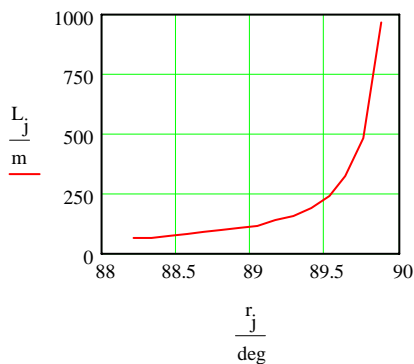


**Fig. 30** Length  $L$  vs grazing angle  $r$

However, it is instructive to remember the magnification feature of Fig. 26 that derives from Eq. (9). To put give the parameter a figure of merit, consider how grating length grows with angle of grazing exodus for a fixed diameter of secondary mirror. In the example of Fig. 30, the secondary mirror is modeled to be 2 meters. Kilometer scale length can be achieved at grazing exodus of 89.881°. We define the effective efficiency  $e_f$  as the product of POG length  $L$  and the efficiency,  $e$ , divided by the mirror diameter  $D$ .

$$(13) \quad e_f = \frac{eL}{D}$$

It might seem that lowering of efficiency by pushing the grazing exodus to maximize length would defeat the goal of increasing flux collection. However, the available flux keeps growing. As shown in the graphs of Fig. 31, even while efficiency drops toward zero, gain keeps growing. Despite the efficiency loss with increases in grazing angle, the benefit of increasing POG length is not overridden.

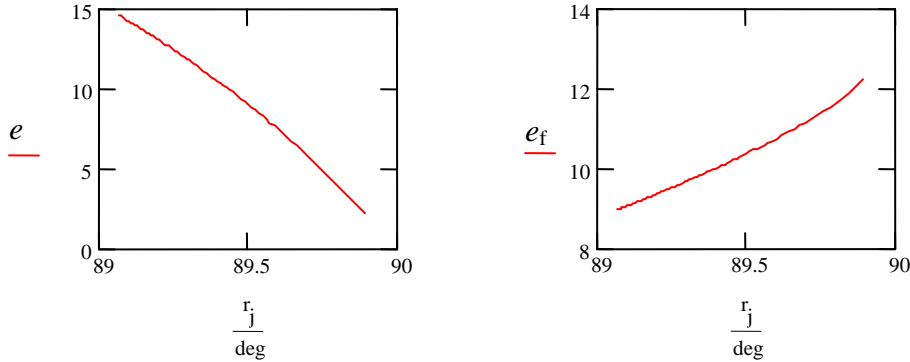


**Fig. 31** Comparison of loss of efficiency with continuing gain as function of grazing angle

Flux collection is also controlled by the rate of precession. For precession along the Great Circle the transit rate  $\omega$  is 15 arcseconds of angle per second of time. In this case, if the meridian is tagged as time  $t = 0$ , the angle of incidence  $i$  upon the POG can be calculated as  $i = \omega t$ . Solving for  $t$  in the Grating Equation we have:

$$(14) \quad t = \frac{a \sin \left[ \frac{(n\lambda - p \sin(r))}{p} \right]}{\omega}$$

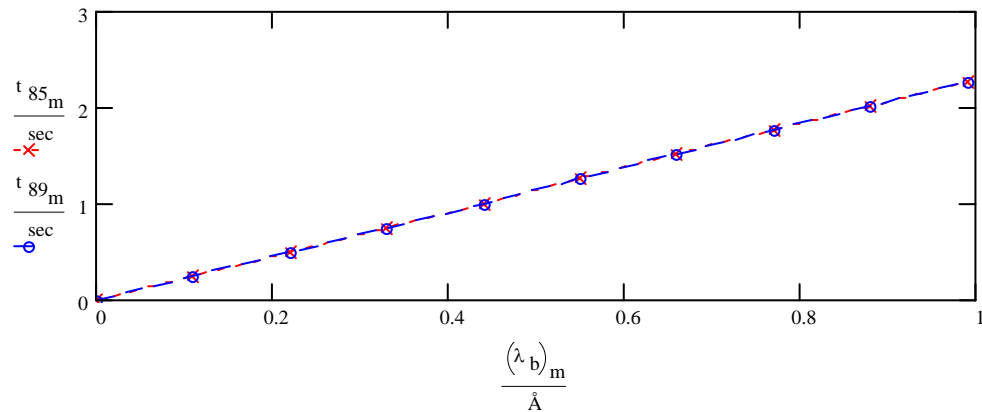


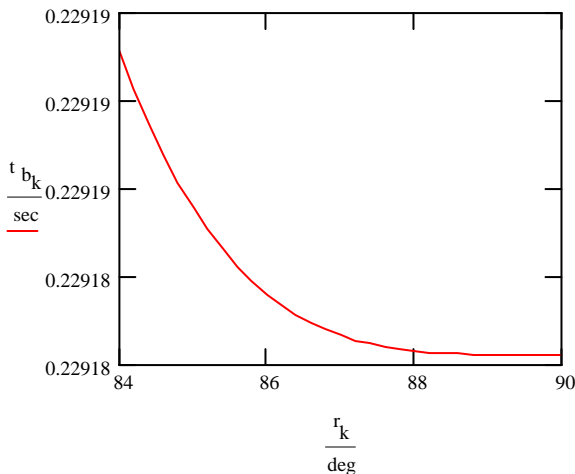
**Fig. 32** Integration times for bandwidths  $\lambda_b < 1 \text{ \AA}$  for  $r = 85^\circ$  and  $r = 89^\circ$

The integration time can then be known from Eq. (15) by bracketing  $\lambda$  in Eq. (14).

$$(15) \quad t_b = \frac{\arcsin\left[\frac{n[\lambda_b + \lambda] - p \sin(r)}{p}\right]}{\omega} - \frac{\arcsin\left[\frac{n\lambda - p \sin(r)}{p}\right]}{\omega}$$

Integration to over wavelength band  $\lambda_b$  can be known by Eq. (15). If the bandwidth is restricted to one discrete wavelength, the integration time is zero. The telescope only produces spectra for sources in precession. In an example graphed in Fig. 32, integration times for wavelength bands from 0 to 1 Å width  $\lambda_b$  are the nearly same for reconstruction angles  $r = 85^\circ$  and  $r = 89^\circ$ . The calculation confirms our earlier published assertion<sup>21</sup> that the worst case integration time for the POG telescope on earth is 2.3 sec per Å.

There is a slight variation over values of  $r$  which is attributable to an increase in spectral resolution as  $r$  increases..



A sample calculation for the case of bandpass 0.1 Å is graphed in Fig. 33. In the diagram below, a narrowly resolved source below will enter and exit from the slit more quickly than a less clearly resolved source above. We conjecture that as resolution goes up with  $r$ , this results in a minor variation in the period of  $t_b$  vs  $r$ .

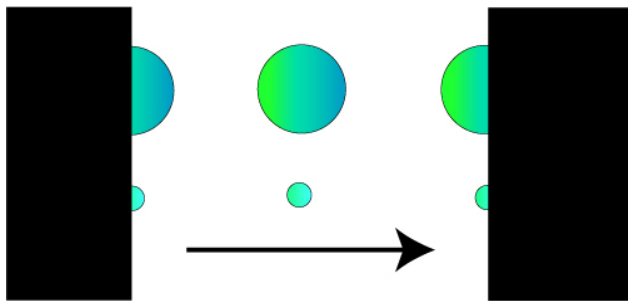


**Fig. 33** Slight variation in integration period

There is a far more pronounced difference in integration times if multiple slits are used at the focal plane of the secondary mirror. An analysis was provided under a consultation with Dr. David Mozurkewich<sup>22</sup> examined precession. To study all angles available to the secondary mirror, Mozurkewich renames  $r$ , the receiving angle, as  $\theta$  the field angle, where nominally,  $(90^\circ - r) = \theta$ . He defines another angle  $\theta_0$  as

$$(16) \quad \cos(\theta_0) = n \frac{\lambda}{p}$$

Now the Grating Equation can be written as

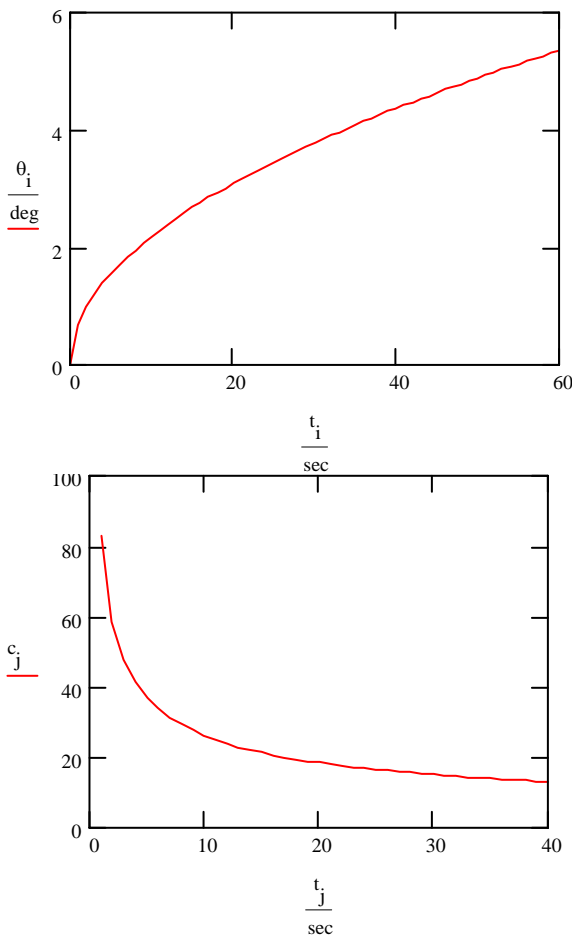
$$(17) \quad \cos(\theta) = \cos(\theta_0) - \sin(\omega t)$$

Refining our parameter  $M$  of Equations (9 & 10), above, to also account for effect of foreshortening at the input, Mozurkewich broadens that definition of magnification. He calls it the compression of the POG which we notate here as  $c$ .

$$(18) \quad c = \frac{\cos(\omega t)}{\sin(\theta)}$$

Equations (17 & 18) can be combined as

$$(19) \quad c = \frac{\cos(\omega t)}{\sqrt{1 - (\cos(\theta_0) - \sin(\omega t))^2}}$$



These equations can be used to demonstrate that the greater the compression, the lower the field angle while at the same time, the lower the field angle, the shorter the integration time. We show sample field angle calculations for a 600 nm grating Fig. 34. The analysis reveals that although there are diminishing returns in compression, overall integration time for all compressions can be equal to all angles traced from the POG, to the mirror and then to the mirror's focal plane. The total integration time with multiple slits at the focal plane of the secondary mirror will be greater than the 2.3 sec/Å minimum as calculated by Eqs. (14 & 15) and graphed in the examples shown in Figs. (32 & 33).

Mozurkewich then asserts a limitation on collection with increases in field-of-view: "...integration time depends only on the field of view of the [secondary mirror] collector and not on the size of the primary grating." He reasons that, "...as the compression of the dittoscope is increased, the speed at which the image moves across the field of view of the collector increases by ...exactly the

**Fig 34** Integration time increases with field-of-view while compression decreases with time.

same factor; at constant field of view, the ratio is independent of compression." To further quote, "A single star is observed for hours, but... the greater the beam compression, the shorter the integration time. The result is the number of photons per bandpass that be detected by a dittoscope is independent of the compression ratio; it depends only on the diameter and field-of-view of the telescope looking at the grating."

Whether the secondary mirror is growing in order to accommodate an increased POG length or the POG length is growing to accommodate an increased secondary mirror diameter is something of a chicken and egg question. Either way, we graphed the dependency in Fig.25. Either parameter could have been plotted on the abscissa.

We are interested in taking an unprecedented number of spectra during an observation cycle, and a long POG with its secondary at grazing exodus is more practical than a large secondary with a small POG, because fewer slits are required at the mirror focal plane than the alternative configurations such as placing a coarse grating in front of a large mirror or skipping the POG in favor of a traditional mirror telescope with a secondary MOS. With a single slit, POG length is fully extensible regardless of mirror size.

The compact field for the spectrograph slits can be shown by considering integration time. For a given field of view at the secondary mirror of a POG, the integration period  $t_p$  as a function of its angle of view from  $r_1$  to  $r_2$  can be calculated by:

$$(20) \quad t_p = \frac{\arcsin\left[\frac{n\lambda - p \sin(r_2)}{p}\right]}{\omega} - \frac{\arcsin\left[\frac{n\lambda - p \sin(r_1)}{p}\right]}{\omega}$$

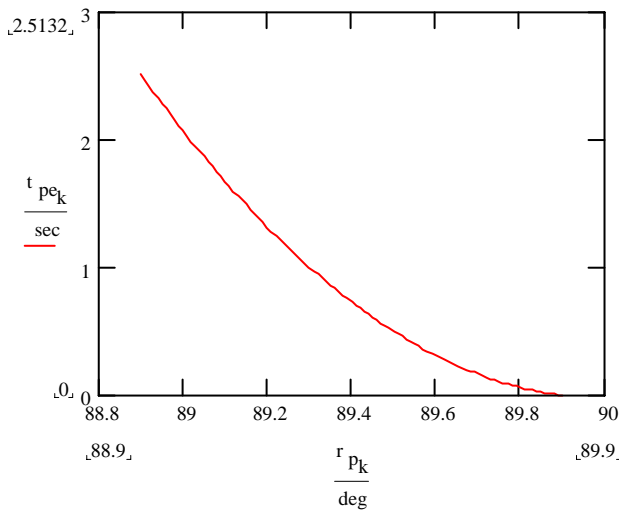


**Fig. 35**  $t_p$  increases by opening the slit over  $1^\circ$

angles of grazing exodus, over a  $1 \text{ \AA}$  bandwidth a single spectrometer slit collects all the light from the secondary mirror that captures it. For  $1/10^{\text{th}}$  the bandwidth, i.e.  $0.1 \text{ \AA}$ , ten secondary spectrometer slits would be needed; for  $0.01 \text{ \AA}$ , 100 slits.

On the other hand, a zenith tube with a  $1^\circ$  field-of-view would integrate for 240 seconds. It would require a separate slit for each resolved pixel to achieve the time domain integration on all sources that precess over  $1^\circ$ . For example, with an angular resolution of 3.6 arc seconds per pixel, that would be 1000 slits. This number is dictated by the angular resolution selected for the telescope and is independent of the spectral resolving power, because a mirror primary telescope relies solely on the performance of the secondary spectrograph to set spectral resolution. The finer the spatial resolution of a zenith tube, the more slits would be required to take meaningful spectra. This approach to MOS has never been taken with zenith tubes or with mirror telescopes in general, because it implies that there would be a spectrometer fiber at every image pixel.

We have shown that at grazing exodus a band of  $1 \text{ \AA}$  can be acquired in a period of 2.3 sec. As it happens, that is nearly equivalent to the period of time it takes for a POG secondary mirror with a  $1^\circ$  field-of-view to project the sky over angles of grazing exodus from  $89.9^\circ$  to  $88.9^\circ$  where the time of the passage of a wavelength across the focal plane is calculated using Eq. (20). In Fig. 35 we show how the field angle changes the integration time when we widen the field-of-view  $\theta$  subtended upon a slit runs from  $0^\circ$  to  $1^\circ$ . At these

One can appreciate the depth of the problem of MOS telescopes from the most recent developments in survey telescope design. The 640 fiber SDSS spectrograph is used only as a follow up procedure after the completion of an SDSS image survey. The goal is to take spectrograms at  $R = 2000$  of 1% of the total catalog. Spectra are restricted to objects identified as of very special interest. Discovery by spectroscopy does not occur as objects are observed. A POG, on the other hand, returns spectra from the first. Even more telling, the forthcoming Large Synoptic Survey Telescope (LSST) does not have a spectrograph, only six band filters that can be swapped in and out over serial cycles of acquisition. Given the gigapixel camera purposed for the LSST, it is not surprising to learn that a fiber at every pixel is not being contemplated.

On the other hand, if a POG at grazing exodus had a comparable 8 m secondary with a  $3^\circ$  field-of-view found on the LSST, the POG would have an effective integration period of the LSST, that is 720 seconds, less POG efficiency losses (perhaps 90%), while collecting the spectrograms of all sources over a line of right ascension that was  $3^\circ$  wide. How many slits would be required? If the mirror was placed at grazing exodus, Eq. (20) predicts that a  $3^\circ$  field-of-view would result in a given wavelength passing over the focal plane in 18.85 seconds, so 9 slits would capture all stars at  $1 \text{ \AA}$ ; 90 slits would capture all stars to  $0.1 \text{ \AA}$ ; and 900 slits would resolve them all at  $0.01 \text{ \AA}$ . These are permanently placed and equally spaced slits rather than custom fiber plates unique to each observation.

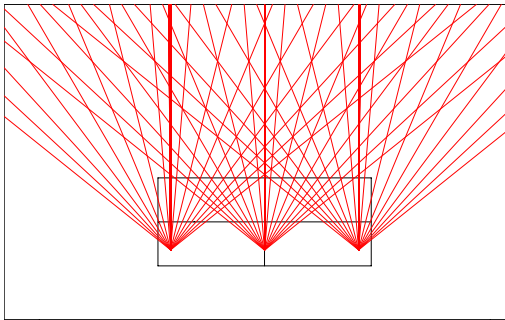


**Fig. 36** Lateral displacement of sources at the focal plane of the spectrograph

The savings in the number of secondary spectrographs is further demonstrated by the fact that all stars are discretely resolved over the latitudinal dimension. At the focal plane array of the spectrograph, stars at different latitudes are discriminated from each other. Fig. 36 taken from a Zemax model shows three sources of the same wavelength that are separated in the firmament by 18 arc seconds laterally from north to south.

That Zemax model, Fig. 37, presumes a very large secondary mirror, 16 m, with a correspondingly large POG, about 400 m. There is only one spectrograph in the model, which would permit extremely fine spectral resolution of bright sources by use of a small slit, or the telescope could survey the entire sky at lower magnitudes with coarser resolving power. The type of spectrograph used in this Zemax model is based on an assembly of large holographic gratings like those of Fig. 20. We note that similar holographic POGs might also overcome the sensitivity restrictions on plane gratings that Mozurkewich has shown are caused by secondary mirror size and placement.

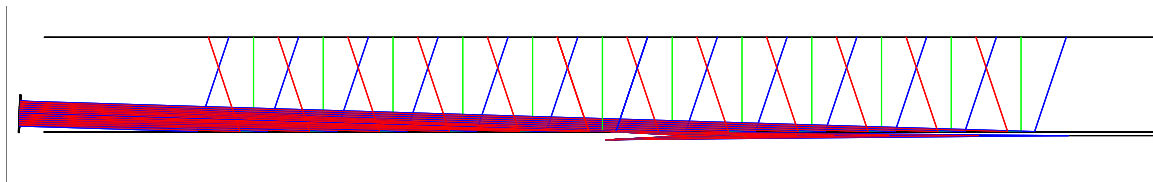


**Fig. 37** Large 400 m POG with 16 m secondary mirror modeled in Zemax

One must allow that comparing mirror primaries with a POG is comparing apples with an orange. A POG sees a fixed wavelength at each angle of incidence, and a spectrum can be acquired only when the stars precess. Without precession, the POG in the grazing exodus configuration cannot take spectra at all, but a mirror primary telescope can. The POG exhibits a complex interlocking set of relationships between precession rate, spectral resolving power and angular resolution that does not correlate with the same parameters for mirror or corrected lens primaries that have little or no chromatic aberration.

One way to appreciate the difference is to compare the performance of POGs on the equator with zenith tubes at the pole. In the latter setting a fixed mirror has indefinite integration time, because the precession is entirely within the field-of-view of the telescope. Mirror zenith tubes have their shortest integration time at the equator. This is also true for the POG, but at the pole, the POG cannot obtain any spectra, because the angle of incidence of the stars barely changes. On the equator, the range of available wavelengths is greatest.

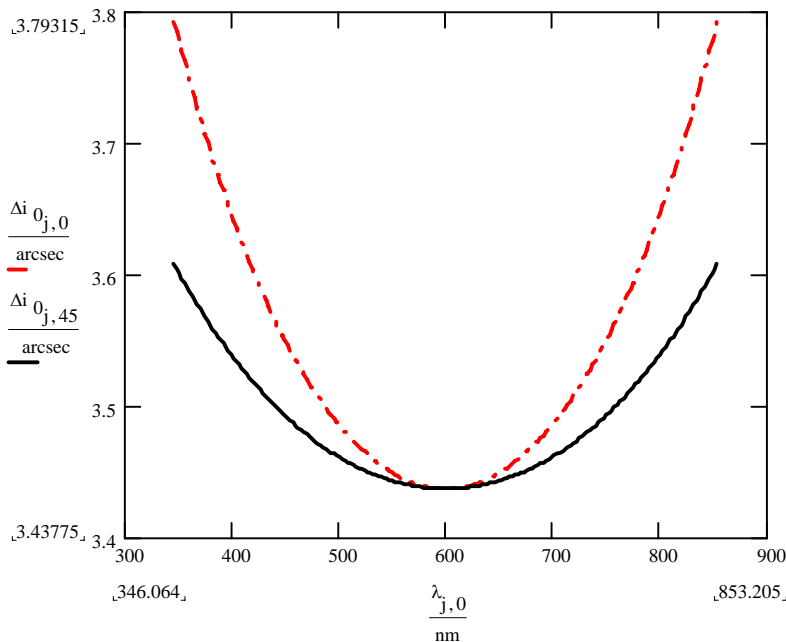


**Fig. 38** Angular resolution for a bandpass of 0.1 Å

about 0.23 sec. The example was calculated for grazing angle of  $r = 88^\circ$ . In this example, the poorest discrimination  $\Delta i$  for our presumed range of  $\lambda$  (400-800 nm) is about 3.7 arc seconds. At the zenith  $\Delta i$  is 3.43775 arc sec. We speculate that the average spacing between stellar targets at this resolving power might be found in the 20<sup>th</sup> magnitude, although specific areas of the sky vary. Like the original POG, there is the risk of ambiguity from overlapping targets when their proximity drops below the  $\Delta i$ . There is a tradeoff with sensitivity when the resolving power is increased. The interplay of parameters will occupy designers and operators.

With a POG, the integration period determines the angular resolution. The longer the integration period is, the coarser is the angular resolution. The finest angular resolution for a fixed time period is at the zenith. Using Eq. (4) we can calculate the relationship for the Great Circle and also for other angles of declination. For example, in Fig. 38 we show both the Great Circle and a latitude  $45^\circ$  for the case where the bandpass created by spacing at the slit is 0.1 Å, and the period of is

### f. Sensitivity and sensibility of the POG

To obtain the effective integration time  $t_{ef}$  when the POG is viewed by a secondary mirror with a field-of-view  $\Theta$  we use Eq. (17) and set  $\theta_0$  to  $90^\circ$  where  $\lambda$  starts at 0. This gives us the complete arc of the sky as received by the secondary. Solving Eq. (17) for  $t_{ef}$  we have

$$(21) \quad t_{ef} = \frac{\arcsin(\cos(\theta_0) - \cos(\theta_0 + \Theta))}{\omega}$$

As Mozurkewich contends, this proves to be equivalent to the integration time of the secondary mirror with exactly same field-of-view. The integration time is graphed in Fig. (39) for a field-of-view  $\Theta$  up to  $3^\circ$ .

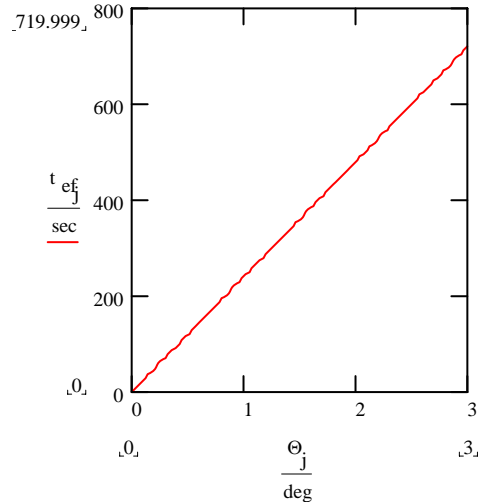


**Fig. 39** POG's effective integration time

This equivalence between a POG and a conventional telescope is a convenient measure, since allows for a sensitivity estimate based solely on the size and field-of-view of the secondary mirror.

The effective compression  $c_{ef}$  in terms of integration period can be integrated over time period  $T$  by:

$$(22) \quad c_{ef} = \frac{1}{T} \int_0^T c(t) dt$$

In Fig. (40) we show the compression over time for a configuration producing an initial compression of 1000.

With compression at the secondary mirror as a function of time we can calculate the number of photons that are collected by the secondary:

$$(23) \quad N = \eta N_0 D^2 c_{ef}$$

Where  $N_0$  is the rate at which the photons are incident upon the grating

$\eta$  is the overall efficiency

$D$  is the diameter of the secondary mirror (assumed to be square)

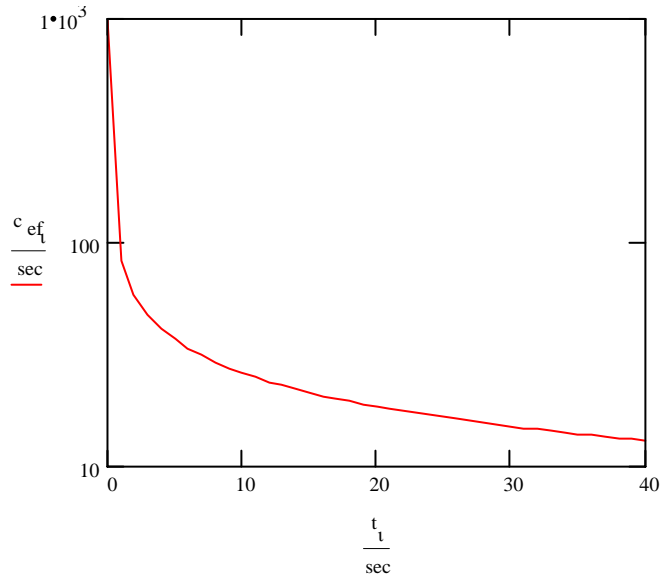


**Fig. 40** POG compression over time from  $c_{ef} = 1000$

Mozurkewich made a calculation for a version of the POG with a 1 square meter secondary mirror having a field-of-view of  $1^\circ$  with. The efficiency of the POG was set at 10%, a conservative figure. PCGrate would suggest 15%, and we have shown by Eq (13)

item	value
atmosphere throughput	90.00%
grating efficiency	10.00%
secondary mirror reflectance (2 mirrors)	96.00%
field slicer throughput	90.00%
spectrograph throughput	83.00%
detector quantum efficiency	80.00%
Total throughput	5.20%
Observing wavelength	650 nm
spectral resolving power	100,000
POG length	100 m
secondary mirror area	$1 \text{ m}^2$
secondary field of view	$1^\circ$
effective integration time	240 sec
stellar magnitude	20

**Table 2** POG throughput and sensitivity estimate

and Fig. (31) that the increase grating length the accompanies the increase in the receiving angle  $r$  counteracts the loss of efficiency as grazing approaches the grating plane. Be that as it may, this prediction for a 10% efficiency POG is given in Table 2.

A s/n of 10 can be achieved with stars a little fainter than magnitude 20 while s/n of 100 could be achieved with stars a two magnitudes brighter. Of course, lowering the spectral resolution will increase sensitivity. Spectra could be taken of objects as faint as magnitude 26 At s/n of 10 and  $R = 1000$ .

One could question the sensibility of building the POG telescope when its cost effectiveness must be compete with conventional telescopes which are now providing comparable sensitivity. However, it helps to rate the potential of MOS. We can estimate how many stars could have their spectra taken by using a table of stars visible in one night of observation. We use Table 3 supplied by cartographer, Richard Monkhouse.

Magnitude	Example	Stars / degree <sup>2</sup>	$1^\circ \times 90^\circ$	Stars to this magnitude
-1.42	Sirius			1
6.5	Yale catalog			6,500
10.5	Hipparchus cat.	3	270	110,000
12	3" scope	12	1,080	500,000
13	6" scope	25	2,250	1,000,000
14	10" scope	60	5,400	2,500,000
15.5		300	27,000	10,000,000
20.5		30,000	2,700,000	1,000,000,000
23	Best scope	300,000	27,000,000	10,000,000,000

**Table 3** Spectrographic survey capability of the POG as a function of stellar magnitudes

Referring to the  $1^\circ \times 90^\circ$  column, one could assert that the POG quantified for sensitivity by the values in Table 2 could catalog twice as many stars to  $R = 100,000$  in one night as the SDSS can hope to survey in a decade at one fiftieth the resolving power.

#### 4. Experimentation

Despite its evident simplicity, the incorporation of a secondary spectrometer into a POG telescope does not appear in the literature prior to our initial suggestion in 2001. After our formal 2002 disclosure, reasons were advanced for a POG astronomical telescope to fail, but the secondary spectrometer and its follow-on data reduction as per Sections 2b and 2c, above, were not among the anticipated show stoppers. Even after several years of professional scrutiny by numerous audiences and juries, qualified experts did not argue against the predictions we were making about double diffraction. This tacit endorsement notwithstanding, we know of no attempt to test our claims through experiment. Therefore, a primary experimental goal for this Phase I project was to perform an empirical demonstration. We can now report experimental proof that a secondary spectrometer does spatially disambiguate a source from its neighbors by spectral selection.

Correspondents and jury reviewers did express skepticism about the viability of the grazing exodus configuration with regard to grating efficiency and flatness tolerances. We can now provide some empirical evidence to justify the continued study of our approach in the face of these related concerns. They are not fatal.

##### a. Angular and spectral resolution

Our bench set-up, Fig. 41 consisted of the grating, a 50 mm Nikon camera lens, and a fiber fed spectrometer, the Ocean Optics USB4000 running under the Spectra Suite JAVA program. The spectrometer was tuned to read from 400 – 700 nm with a nominal resolution of 0.5 nm. We co-mounted a color CCD camera with the distal fiber tip to facilitate alignment. Broadband halogen white light sources were assembled from common gallery lighting fixtures. A photometer gave readings of the incident flux.

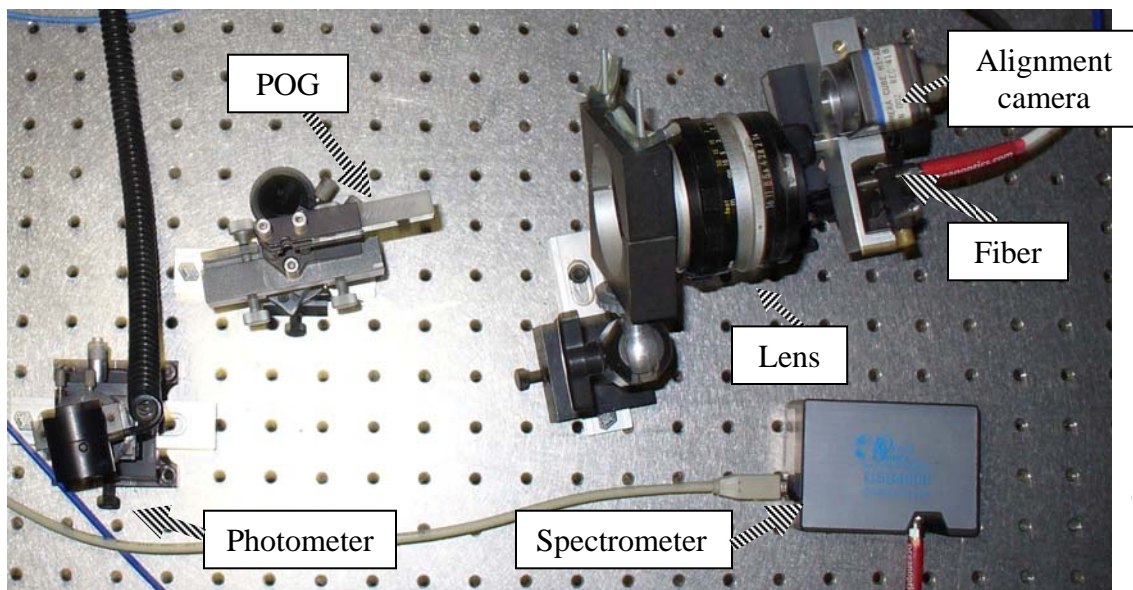
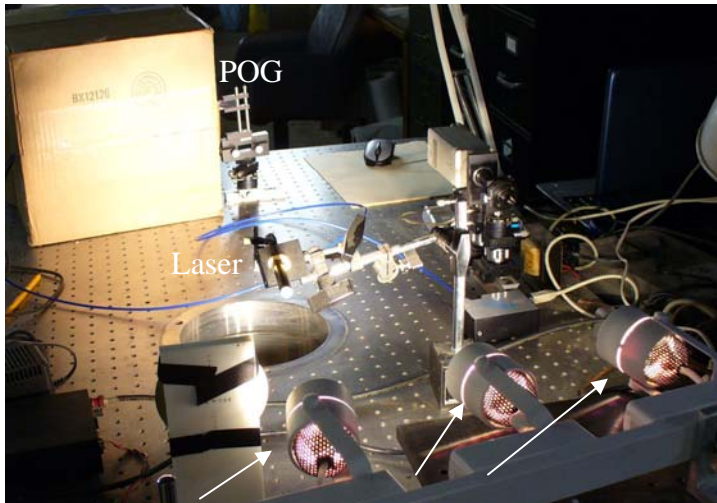


**Fig. 41** 50 mm POG with fiber fed spectrometer, alignment camera and photometer

We selected a 12.7 x 50 mm rectangular diffraction grating. We did not make our first primary objective, as Isaac Newton did. (Newton's was comparable in size.) We used an off-the-shelf 1800 lines/mm Optometrics No. 5-2407 replicated holographic grating optimized for grazing incidence, typically used for tuning lasers. The unit we obtained had an unusually thick 300 nm coat of aluminum for use with high power lasers. Being holographic, the grooves are presumed to be sinusoidal without favoring a direction for the receiver. The manufacturer estimated the groove depth to be around 250 nm.



Halogen white light sources

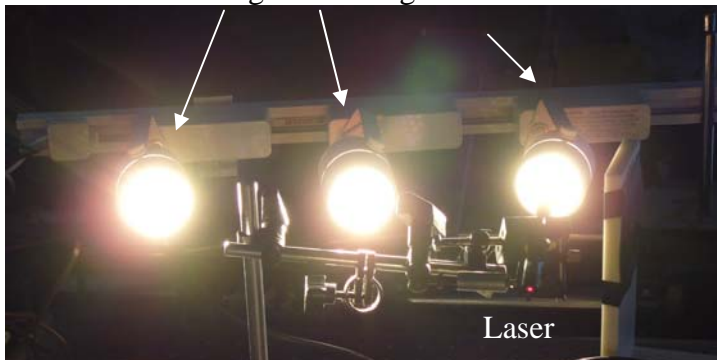


**Fig. 42** Bench top – three white sources and a laser

In order to fit all components, including the sources, on our small breadboard optical bench, the halogen fixtures were placed at 1 m from the POG. Three white light sources and an embedded laser pointer of nominal 650 nm (tested 648.5 nm) were superimposed over one source. The bench top is shown in the upper frame of Fig. 42 while the sources with the embedded laser illumination appear below. The lens and fiber were shielded from the illumination inside a box. The initial test demonstrated the correlation of angle with wavelength for the three sources, and the wavelength of the laser was clearly distinguished as per the spectrogram of Fig. 43.

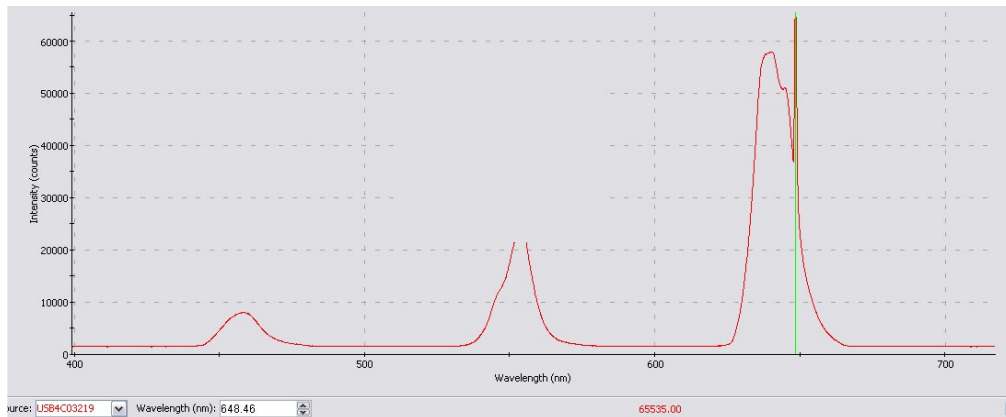


**Fig. 43** The first read-out. A laser is embedded in the red at 650 nm.

The proximity of our artificial stars precluded radiating plane waves without collimating optics. We elected to move the sources to a separate table spaced 5 m across the room in order to flatten the waves. Adjustments were monitored with binoculars, Fig. 44.



**Fig. 44** Three artificial stars at five meters

At this range, the sources were at a narrower angular displacement, and the spectrogram shows this distinction with sharper spikes from full spectrum sources, Fig. 45. The differences in amplitudes were apparently caused by displacements on the non-diffraction axis, i.e., the lens focused light from different latitudes above and below the single fiber.

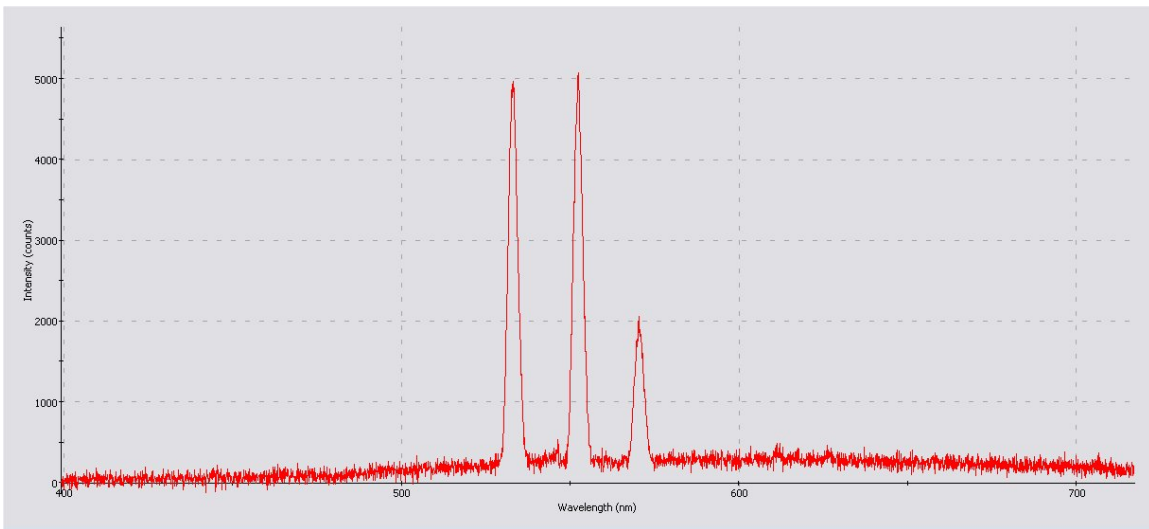


**Fig. 45** Spectrogram of three sources - one on right of slightly different “latitude.”

To study how distance of a source to the POG affected the slope of a detected spike, a tractor was parked outside of the laboratory, 100 feet from the POG, and headlights were used as sources. See Fig. 46. The photograph of the tractor was taken from behind the POG, and the POG's backside is visible here as an occluding rectangle. The spikes were sharper, as expected. One headlight was detected clearly. The other was misaligned and is



**Fig. 46** Refined spikes at 100 feet:  
Top- Sources seen from behind POG  
Middle – Daylight; Bottom - Night

less visible in the spectrogram. When acquired in daylight, the spectrogram shows other sources at other angles. The experiment is instructive, not only in showing that sources are more sharply delineated with distance, but also with regard to applications of a POG telescope might have in hyper spectral terrestrial surveys. When the target was acquired in the dark of night, the misaligned headlight is the only other source and appears as a tiny excursion to the right of the well aligned headlight.

A laser produces a nominal plane wave, anticipating how precisely starlight will be discriminated once the instrument is grown to a scale suitable for astronomy. Another way to compare a plane wave with the spherical wave approximation of our bench at 5 m is seen in Fig. 47. Here the 650 nm laser pointer is positioned between two broad band sources at the 5 m stand-off documented in Fig. 44.

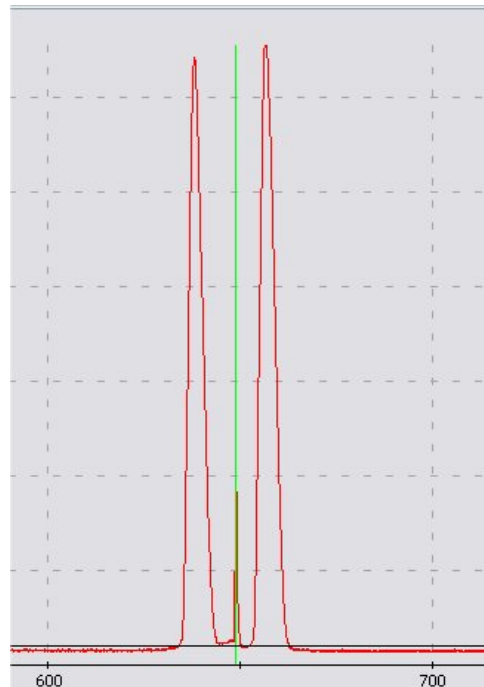


**Fig. 47** A laser's plane wave in center

We settled on a 5 m stand-off for a single halogen “artificial star” which was mounted on a lathe bed driven by a worm gear and read out on a Veeder Root type of mechanical counter nominally accurate to 0.01 inch.

inches	deg	arc sec	nm	$\Delta\lambda$	
0.00		54.28	555.51		
0.05			555.49	0.012	discarded
0.10	0.015	0.00	555.35	0.14	
0.15	0.015	54.28	555.21	0.14	
0.20	0.015	108.56	555.09	0.12	
0.25	0.015	162.84	554.95	0.14	
0.30	0.015	217.12	554.81	0.14	
0.35	0.015	271.40	554.69	0.12	
0.40	0.015	325.68	554.56	0.13	
0.45	0.015	379.96	554.42	0.14	
0.50	0.015	434.24	554.28	0.14	
0.55	0.015	488.52	554.15	0.13	
0.60	0.015	542.80	554.01	0.14	
0.65	0.015	597.08	553.87	0.14	
0.70	0.015	651.36	553.74	0.13	
0.75	0.015	705.64	553.6	0.14	
0.80	0.015	759.92	553.47	0.13	
0.85	0.015	814.20	553.33	0.14	
			Avg.	0.135	

We advanced the source in a direction parallel to the POG for 0.05 inch per sample. We could then calculate angles of incidence  $i$  with this standoff as a function of the translation following

$$(24) \quad i = \arctan\left(\frac{x}{d}\right)$$

where  $x$  is translation on lathe bed  
 $d$  is distance from “star” to POG

The center band for our POG of 1800 1/mm is 555.55 nm. There was some whiplash in the mechanical system, and the first readings were discounted. The experimental results are listed as Table 4. A sample spike from the set of spectrograms is shown in Fig. 48. The resulting displacements conform to predictions consistent with Eq. (4).

**Table 4** Changes in wavelength in 0.015° steps

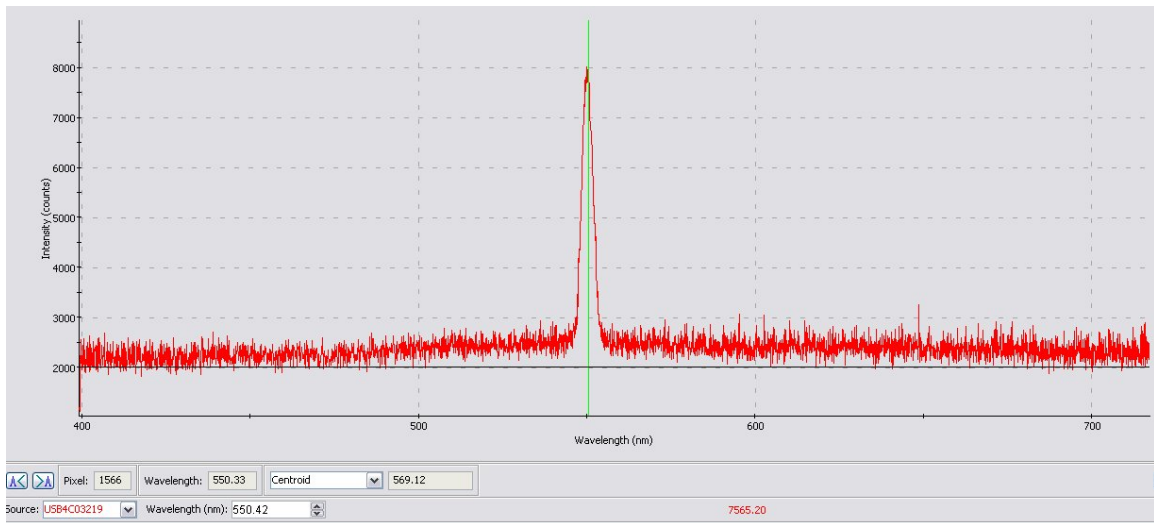


**Fig. 48** Spectrograph of green portion of “artificial star” centered at 555.55 nm

We transposed the table to another position and took a second set of readings near to 552 nm. The results are reported in Table 5. The slight increase in the average increment of change of the wavelengths in Table 5 compared with average in Table 4 is consistent with the prediction of Fig. 38. This is to say, the resolution of the telescope is greatest at

the zenith. The tradeoff is with integration time, a factor that is not being measured in these experiments where spectrometer integration time was on the order of milliseconds.

inches	deg	nm	$\Delta\lambda$
0.00	0.015	552.62	
0.05	0.015	552.51	0.11 discarded
0.10	0.015	552.36	0.15
0.15	0.015	552.23	0.13
0.20	0.015	552.08	0.15
0.25	0.015	551.94	0.14
0.30	0.015	551.79	0.15
0.35	0.015	551.64	0.15
0.40	0.015	551.49	0.15
0.45	0.015	551.35	0.14
0.50	0.015	551.21	0.14
0.55	0.015	551.06	0.15
0.60	0.015	550.91	0.15
0.65	0.015	550.76	0.15
0.70	0.015	550.61	0.15
0.75	0.015	550.48	0.13
0.80	0.015	550.32	0.16
0.85	0.015	550.18	0.14
0.90	0.015	550.03	0.15
0.95	0.015	549.9	0.13
1.00	0.015	549.76	0.14
Total field	0.286		
Average change in nm			0.145
total range in nm		2.440	

**Table 5.** Extended readings toward blue

We found that the method of disambiguating broadband sources using a secondary spectrometer is so robust to that we were able to experiment in room light. Working in daylight accounts for the noise floor seen in Fig. 48, as contrasted with Figs 46 and 47 which were taken at night. As measured by a photometer, the flux arriving at the POG from each “artificial star” at 5 m distance was 178.6  $\mu\text{W}$  per cm at full bandwidth or nearly 900  $\mu\text{W}$  at full bandwidth over the entire face of the 50 mm POG. Of course, this is a more light than celestial objects, but the POG can be scaled up as needed for an astronomical telescope.

We have collected a substantial amount of data from our bench, and we hope to have an opportunity to prepare it for publication in the near future. We leave the reader here with this corroboration by experiment of the underlying principle behind the telescope.

The experiment merely proves that the double diffraction method which combines a POG with a secondary spectrometer does produce a correlation of wavelength to angle. Without the secondary spectrometer, the image recorded by our alignment camera was a hodgepodge of wavelengths from broadband sources. The laser can be seen as a red point in Fig. 49, adjusted into a position below the “stars” in this photograph to facilitate its discrimination. In Figs. 43 and 47 the laser was necessarily lodged inside the blur made by the full bandwidth sources, since the fiber fed spectrometer could only detect one “latitude.”

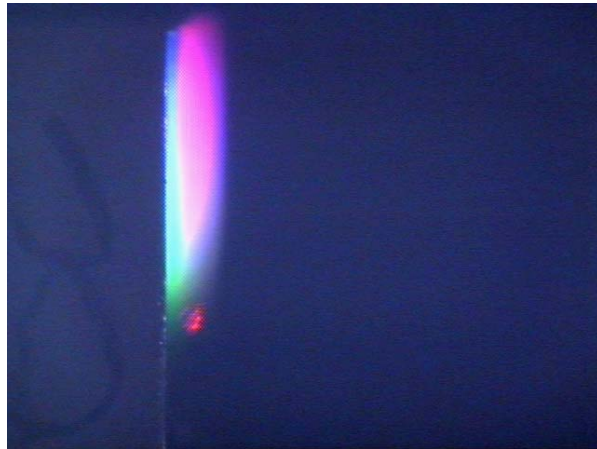


**Fig. 49** An image from the alignment camera

We found that the method of disambiguating broadband sources using a secondary

**b. POG efficiency**

Our efficiency test bench is diagrammed in the rendering of Fig. 50. A 635 nm laser was expanded by a Powell lens (which linearizes flux distribution), collimated with an F/1 laser printer lens, and directed to the test grating which was on a micro-positioning rotation platform which

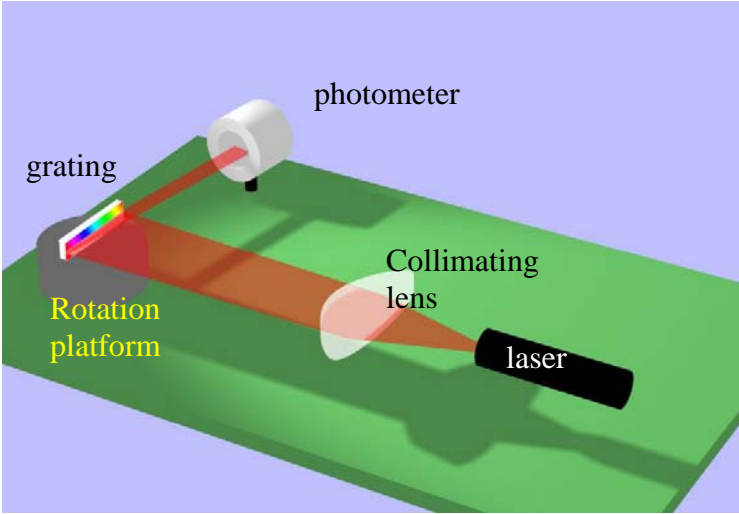


**Fig. 50** Efficiency test bench diagram

gave us readings for the incident angle. The diffracted light was measured at a photometer and compared with the flux collected using the same photometer in a series of readings spanning the entire width of the grating. Incident angle was correlated to the receiving angle using the grating equation. The efficiency was the ratio of the flux striking the grating to the flux picked up by the photometer.

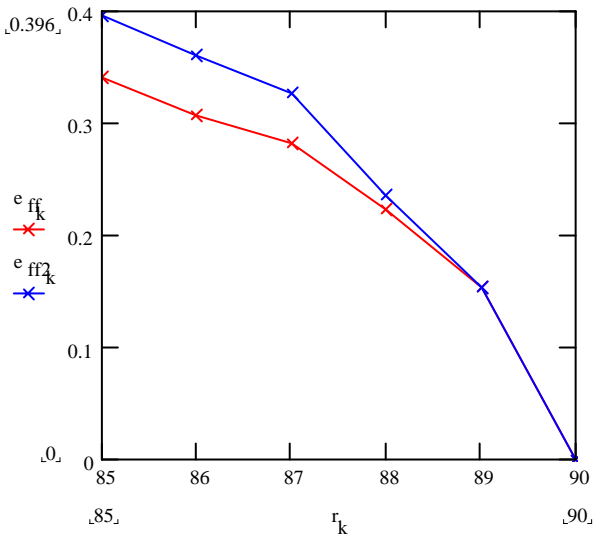


**Fig. 51** Measured efficiency TM wave

The Optometrics grating used in the experiments reported in Section 4a, above, showed efficiencies resembling performance predicted by PCGrate as shown in Fig. 29 of Section 3e. We tested the grating twice as recorded in Fig. 51. The diode laser was polarized and the test was for the transverse magnetic polarization where efficiency is optimized.

We also tested blazed gratings, but they were 1200 lines/mm. The 635 nm laser's first-order was not at grazing exodus. Efficiencies of 50% were possible in the first-order where it did reconstruct.

We also tested blazed gratings, but they were

### c. Flatness tolerance

In order to compare the tolerance reflection with diffraction, we used a defectively mounted embossed plastic grating in both reflection and diffraction modes. This was easily accomplished by turning the grating  $90^\circ$  and viewing the spectrometer slit illuminating the grating. The comparison can be seen in Fig. 52.

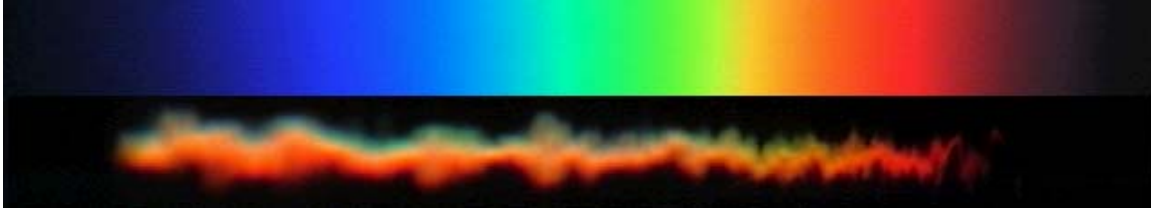


**Fig. 52** Comparison of dispersion (above) and reflection (below) with identical flatness

A very shallow residual spectrum can be seen in the reflection image in the lower frame of Fig. 52. The shallow spectrum is perpendicular to the long reflection of the grating slit, indicating that this is a reflection grating that has been rotated  $90^\circ$ . The result that matters is along the axis of grazing exodus, the considerable widths of both images. While the spectrum above is seemingly perfectly smooth, the reflection is distorted by the uneven surface. Both images exhibit perspective foreshortening, because the images were taken with an ordinary lens, rather than a telecentric lens or parabolic mirror.

We can see how the effects of an uneven grating are ameliorated as the grating goes into a grazing exodus configuration in Fig. 53.

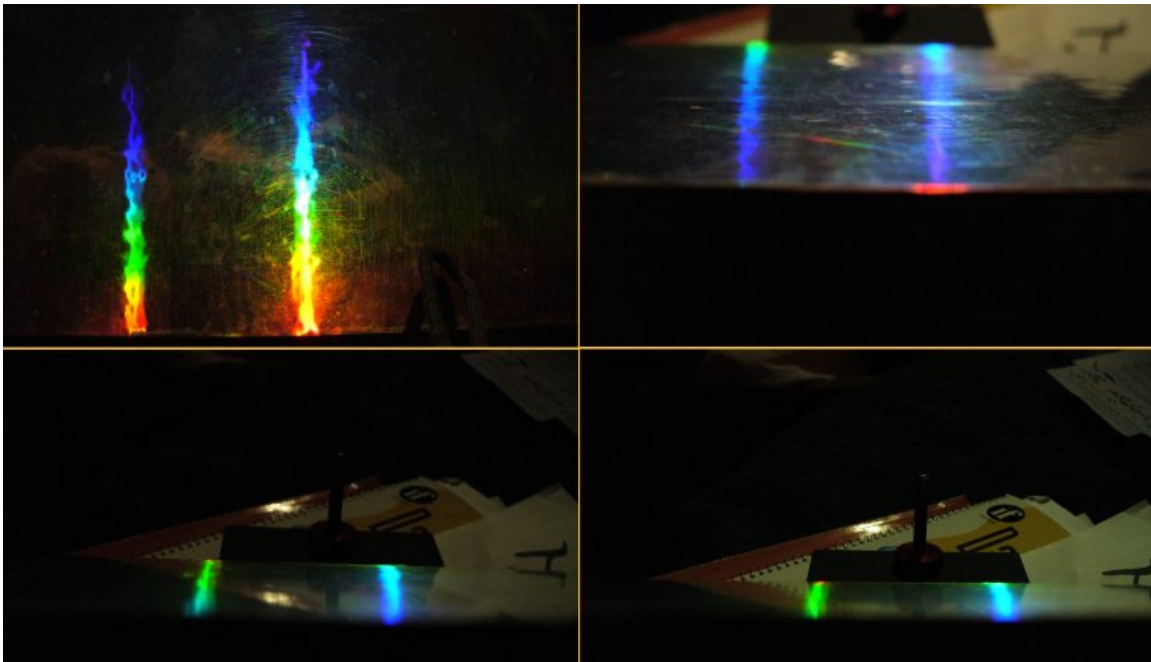


**Fig. 53** An uneven grating is rotated into the grazing exodus configuration

## 5. Recommendations

There has not been a fundamental rethinking of telescope primary objectives in well over three centuries, and at the same time, there has been a great deal of thought put into the two types of primary objective that have been implemented during that long period. A lot less is understood about dispersion than refraction and reflection, so fundamental research is needed to clarify the physical optics needed to refine a POG telescope. Holography and microstructure replication are relatively recent areas of study.

We have learned in course of this investigation that a plane grating achieves its greatest magnification at an angle of grazing exodus where its integration time is shortest and its efficiency is lowest. An improvement in performance may be achieved using a holographic POG. As it happens, in the course of designing a secondary spectrometer, we examined holographic gratings which are extensible to the POG itself. The hologram has the advantage of lifting the reconstruction of the incident wave above the grating plane while also focusing the light in the same manner as a secondary mirror. Indeed, the lunar observatory we propose assumes such a holographic POG so that it can discriminate between lateral sources. We can model a variety of POGs with different types of holographic pattern. We might begin with a variable pitch grating that has straight line grooves. For example, such a grating could be embossed on a gossamer membrane using a drum embosser that was gradually heated to expand its diameter. The use of ribbon shaped gratings that take advantage of recent developments in microstructure embossing could lead to airborne and space deployed telescopes of unprecedented power.

Because diffraction gratings have never been extended to the physical limits required to implement the POG telescope, there were no ready references at hand when we looked at flatness tolerances. The result of our inquiry was counter intuitive and diverged from the informal guidance we received from experts. However, uncharted territory still remains in dealing with stochastic errors in flatness. This parameter can be approached statistically. An even more vexing issue is pitch phase error. Our analysis suggests that grazing angles aggravate errors in this parameter. We must develop a comprehensive theory to characterize the error, test it, and initiate the materials science research needed to provide robust substrates that can control pitch spacing.

We have been warned to be prepared for a long battle to win acceptance. Just as Descartes faulted Mersenne, we have been advised by leading authorities to put our ideas aside. We have been told repeatedly that conventional telescopes adequately serve astronomers. In light of these dismissals, the first recommendation we make to ourselves is to not give up, with or without approbation or funding. This inventor is familiar with working alone without support and has a personal history of having his ideas rediscovered decades after he first broached them. Notably he invented a process for computer animation in 1976 which he called Pantomation. About twenty years later it became a widely practiced technology called "motion capture." This year, 2007, he was asked to restore his 1974 animation facility for use by a contemporary artist working on an IMAX 70 mm film production. There is often is a latency between invention and recognition. We won't let a preoccupation with reality stifle our imagination.<sup>23</sup>

## References

---

<sup>1</sup> <http://home.earthlink.net/~scan3d/html/Dittoscope.html>

<sup>2</sup> <http://www.sdss.org/>

<sup>3</sup> <http://www.maui.afmc.af.mil/>

<sup>4</sup> <http://www.stsci.edu/hst/>

<sup>5</sup> <http://www.jwst.nasa.gov/>

<sup>6</sup> Peterson & Agnes, "How the Mass Of Large Gossamer Optical Telescopes Scales with Size and Disturbance Environment," *Structures, Structural Dynamics and Materials*, AIAA 2007-1813, p. 13

- In his oral conference presentation Peterson asserted verbally that  $1.1 \text{ kg/m}^2$  is the greatest allowable primary objective aerial mass, but that such an option would require "a miracle material not yet known." Nonetheless, he used this figure to design a large scale space mirror.

<sup>7</sup> Newman et al, "Mass-producing spectra: The SDSS spectrographic system," *Ground-based Instrumentation for Astronomy, Proc. SPIE*, V. 5492, pp. 533-544 (2004)

<sup>8</sup> Ge, Mahadevan, et al, "All Sky Doppler Extrasolar Planet Surveys with a Multi-object Dispersed Fixed-delay Interferometer," *Scientific Frontiers in Research on Extrasolar Planets*, ASP Conference Series, V. Vol. 294, 573, 2003 see <http://www.astro.ufl.edu/et/index.html>

<sup>9</sup> <http://www.astro.lu.se/~torben/euro50/>

<sup>10</sup> <http://www.eso.org/projects/owl/>

<sup>11</sup> <http://www.eso.org/projects/e-elt/>

<sup>12</sup> Ditto and Friedman, "Gossamer Membrane Telescope," *Structures, Structural Dynamics and Materials*, AIAA 2007-1816

<sup>13</sup> Lindler, Flint & Rankin, Design Equations & System Implications of Thin Film Membrane Mirrors and Windows, *Structures, Structural Dynamics and Materials*, AIAA 2007-1815

- "As ... shown in the full paper, this rim design could be significantly lightweighted [*sic*] to about  $1 \text{ kg/m}^2$  and still maintain its primary coupled system frequency above 100Hz."

<sup>14</sup> Thomas Ditto, "Kilometer scale primary objective telescope with no moving parts," *Large Ground-based Telescopes, Proc. SPIE*, 2002, V. 4837, p. 652, Fig 7, eq. (3)

<sup>15</sup> <http://niac.usra.edu/files/library/meetings/fellows/mar07/1350Ritter.pdf>

<sup>16</sup> [http://niac.usra.edu/files/studies/final\\_report/7Hoyt.pdf](http://niac.usra.edu/files/studies/final_report/7Hoyt.pdf)

<sup>17</sup> Dragovan, Tolomeo, et al, "Design and test of prototype DART system," *Highly Innovative Space Telescope Concepts, Proc. SPIE*, V.4849, pp. 8 – 16 (2002)

<sup>18</sup> [http://niac.usra.edu/files/studies/final\\_report/1006Angel.pdf](http://niac.usra.edu/files/studies/final_report/1006Angel.pdf)

<sup>19</sup> Phillips et al, "Grazing incidence holograms and system and method for producing the same," US Patent 6,151,142, Nov. 21, 2000

<sup>20</sup> Ditto and Friedman, AIAA, *op.cit.*

<sup>21</sup> Tom Ditto, "The Dittoscope," *Future Giant Telescopes. Proc. SPIE*, 2002, V. 4840, pp. 586-597, Section 3.1

<sup>22</sup> David Mozurkewich, "The Sensitivity of a Spectroscopic Telescope with a Diffraction Grating Primary," Seabrook Engineering, Seabrook, MD 20706-3108, Private Communication, January 8, 2007

<sup>23</sup> The NIAC motto